Available online at www.sciencedirect.com
SCIENCE DIRECT®
Geochimica et Cosmochimica Acta 70 (2006) 1616–1635
Geochimica
www.elsevier.com/locate/gca

Composition of groundwaters associated with porphyry-Cu deposits, Atacama Desert, Chile: Elemental and isotopic constraints on water sources and water–rock reactions

Matthew I. Leybourne [a,*], Eion M. Cameron [b]

[a] Geosciences Department, University of Texas at Dallas, Richardson, TX 75083-0688, USA
[b] Eion Cameron Geochemical Inc., 865 Spruce Ridge Road, Carp, Ont., Canada K0A 1L0

Received 20 January 2005; accepted in revised form 5 December 2005

Abstract

Groundwaters were collected around the Spence porphyry copper deposit, Atacama Desert, northern Chile, to study water-porphyry copper ore bodies interaction and test hypotheses regarding transport of metals through thick overburden leading to the formation of soil geochemical anomalies. The deposit contains 400 Mt of 1% Cu and is completely buried by piedmont gravels of Miocene age. Groundwaters were recovered from the eastern up hydraulic gradient (upflow) margin of the Spence deposit, from within the deposit, and for two kilometers down flow from the deposit. Water table depths decrease from 90 m at the upflow margin to 30 m 1.5 km down flow. Groundwaters at the Spence deposit are compositionally variable with those upflow of the deposit characterized by relatively low salinities (900–7000 mg/L) and Na^+–SO_4^{2-}-type compositions. These waters have compositions and stable isotope values similar to regional groundwaters recovered elsewhere in the Atacama Desert of Northern Chile. In contrast, groundwaters recovered within and down flow of the deposit range in salinity from 10,000 to 55,000 mg/L (one groundwater at 145,000 mg/L) and are dominantly Na^+–Cl^--type waters. Dissolved sulfate values are, however, elevated compared to upflow waters, and $\delta^{34}S_{CDT}$ decreases into the deposit (from >4‰ to 2‰), consistent with increasing influence of sulfur derived from oxidation of sulfide minerals within the deposit. The increase in salinity and conservative tracers (Cl^-, Br^-, Li^+, and Na^+) and the relationship between oxygen and hydrogen isotopes suggests that in addition to water–rock reactions within the deposit, most of the compositional variation can be explained by groundwater mixing (with perhaps a minor role for evaporation). A groundwater-mixing scenario implies a deeper, more saline groundwater source mixing with the less saline regional groundwater-flow system. Flow of deeper, more saline groundwater along pre-existing structures has important implications for geochemical exploration and metal-transport models.

1. Introduction

Demands on ground and surface water resources are increasing worldwide in arid and hyper-arid regions (UN Commission on Sustainable Development, 1997; Meigh et al., 1999). The Atacama Desert of northern Chile, the driest region on Earth, receives <10 mm/a rainfall, with scattered population centers relying on a small number of rivers fed by recharge in the high Andes and on groundwater (Magaritz et al., 1989). In the hyperarid climate of the Atacama Desert, there are competing interests for limited water resources; as drinking water, for the large Cu-extraction industry and migratory species (Romero, 2002; Núñez and Grosjean, 2003). As shown in this study and elsewhere (Magaritz et al., 1989, 1990; Alpers and Whittemore, 1990; Aravena and Suzuki, 1990; Carmona et al., 2000; Risacher et al., 2003; Romero et al., 2003), ground and surface waters in northern Chile are highly variable in concentration of total dissolved solutes. The origins of both dilute and saline waters in Atacama Desert aquifers and the dissolved constituents of

* Corresponding author.
E-mail address: mleybo@utdallas.edu (M.I. Leybourne).

0016-7037/$ - see front matter © 2005 Elsevier Inc. All rights reserved.
doi:10.1016/j.gca.2005.12.003

these waters remains poorly understood. Areas of uncertainty include the timing and location of recharge (i.e., modern recharge in the high Andes vs recharge at lower elevation during past pluvial periods) and the sources of solutes to deeper brines (dissolution of old evaporites, downward migration from brine lakes in many of the closed basins, dissolution of surface salts, water–rock modification of connate water) (Risacher et al., 2003).

Northern Chile hosts some of the largest porphyry-copper deposits in the world (e.g., Chuquicamata, La Escondida; Fig. 1); continued exploration for copper resources requires extending the search for undiscovered mineralization into areas of thick cover (Cameron et al., 2004). Geochemical exploration for base metal mineralization has, in recent years, focused on the use of partial, or sequential, leaching of soils/sediments overlying the mineralization and these methods are predicated on the observation that commonly significant (high signal/noise) geochemical anomalies are developed over mineralization, in many instances deeply buried (up to 200 m) (Hall et al., 1996; Cameron et al., 2004). Mechanisms that have been postulated to explain these geochemical anomalies include upward diffusion, advection, electrochemical cells, vapor-transport, and seismic pumping (Hamilton, 1999; Cameron et al., 2004).

In this study, we present the results of our research into the composition of groundwater in and around a large porphyry copper deposit (Spence deposit; ~400 Mt of 1% Cu) in the Atacama Desert of northern Chile. The goals of this study are to: (1) determine the origins of the waters and dissolved constituents in this region of the Atacama Desert; (2) determine the controls on the groundwater compositions around the Spence deposit; and (3) establish if there is a geochemical link between groundwaters found in and around a large porphyry copper deposit and anomalies observed in the soils overlying the deposit. The results of this study have implications for: (1) the utilization of groundwater as a resource (i.e., exploitation of fossil water); (2) the development of soil anomalies in arid and hyper-arid climates around the world in terms of both mineral exploration and environmental studies of natural sources of contaminants; and (3) sources of solutes and the mechanisms by which saline fluids are mixed with more dilute groundwater flow.

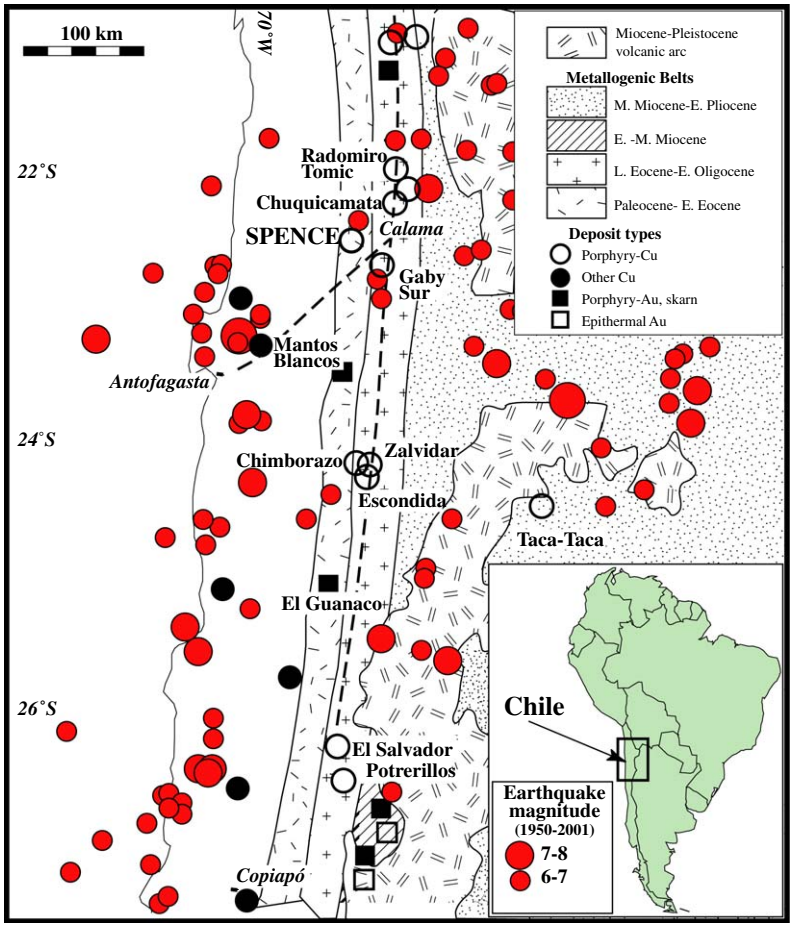

Fig. 1. Regional geology of northern Chile, showing major ore deposits in relation to geologic belts that host them (after Richards et al., 1999). The north-south dashed line is the West Fault discussed in the text. Also shown are the epicenters of major earthquakes (>magnitude 6) from 1950 to 2001 listed in the US Geological Survey database.

2. Geological and hydrological setting

Chile is the largest copper producer in the world, with the bulk of the copper derived from major porphyry deposits that occur within a narrow belt in northern Chile (Fig. 1). The deposits formed from hydrothermal systems derived from Cenozoic continental arc magmatism (Sillitoe, 2000; Tosdal and Richards, 2001). The porphyries were intruded into a collage of igneous, sedimentary, and volcanic rocks accreted to the margin of South America over the period extending from Late Proterozoic to Cretaceous (Ramos, 1988; Richards et al., 1999). Large deposits include Chuquicamata, Escondida, El Salvador, Collahuasi, and Spence (Fig. 1). The deposits occur along major, long-lived fault systems, with many of the deposits located near to the West Fault or Fissure (Fig. 1). Spence is located along a major north-northeast lineament that extends from the coast through the town of Calama (Fig. 1).

Copper in the deposits was enriched by supergene alteration in the mid-Miocene (Chávez, 2000; Cuadra and Rojas, 2001). During supergene alteration, conditions are sufficiently oxidizing at or above the water table that Cu is strongly leached, and subsequently migrates downwards to where conditions become more reducing. During downward migration, Cu is reprecipitated, either as secondary oxides, carbonates, chlorides, sulfates or clays in the oxide zone, or under reducing conditions below the water table, as secondary sulfides (supergene enrichment). Secondary sulfide development typically takes the form of chalcocite and/or covellite replacement of primary bornite and chalcopyrite (Chávez, 2000). Following supergene enrichment, thick piedmont gravels were deposited, as the climate of northern Chile became hyperarid beginning around 14 Ma (Alpers and Brimhall, 1988). The hyperarid climate has reduced the rate of surface erosion to ~1 cm/ka since that time (Alpers and Brimhall, 1988). There have been, however, more pluvial periods during this time (Bobst et al., 2001; Houston and Hart, 2004).

RioChilex discovered Spence in 1996–1997 by grid drilling through piedmont gravels that cover the deposit. The deposit displays a typical supergene-enriched sequence, capped by a leached zone. Reserves recoverable by open-pit mining comprise 50 Mt oxide ore with 1.4% Cu, 200 Mt of enriched sulfide ore with 1.3% Cu, and 150 Mt of primary sulfide ore with 0.6% Cu. Ore is associated with three quartz–feldspar porphyry bodies intruded along a north-northeast axis into andesitic volcanic rocks. The orientation is sub-parallel to the prominent lineament running between the coast and Calama, whose precise location in the basement near Spence has not been determined because of the gravel cover. Intrusions are cut by tourmaline–quartz–sulfide hydrothermal breccias. The irregular leached surface of the deposit is covered by 30–180 m gravels. The gravels thin to the south and elevation generally decreases from east to west, ranging from 1770 m above sea level (masl) in the east to 1695 masl in the west. The deposit is undisturbed except for exploration drilling and construction of a decline tunnel in the southern part of the deposit.

3. Methods

3.1. Sampling techniques

Groundwaters were collected from exploration drill holes using flow-through bailer (1999) and down-hole pump (2000) systems. The bailer consists of a 1-L PVC tube with two stop-valves that permits flow of water through the tube during descent because of the neutral buoyancy of the stop-valves. The valves are closed and the groundwater trapped during retrieval of the bailer. The double-valve pump head is lowered downhole to a depth typically at least 5 m below the water table. The head of water overlying the pump results in groundwater flow into the chamber and up the PVC tubing to the static head level. Nitrogen gas is then forced down one PVC tube into the sample head, resulting in return of groundwater to surface via another PVC tube. Successive samples are taken until steady state conditions are reached for specific conductivity, Eh and pH. Once steady-state conditions are reached, the assumption is made that the system is sampling groundwaters representative of the aquifer at that depth and the sample is taken. Development of the well not only allows greater confidence that the sample represents groundwater flow at that depth, but also serves to decontaminate the sampling apparatus between boreholes. Water samples were tested in situ for pH, Eh, specific conductance (as a measure of salinity), temperature, and dissolved oxygen (DO).

At each sample location, two 125 ml bottles were collected for cation analysis, one sample was filtered to 0.45 μm, using Millipore Sterivex cartridge filters, and the second sample was left unfiltered in order to determine where base metals are sequestered; dissolved or colloidally bound. Cation aliquots were acidified with ultrapure nitric acid. A 125 ml sample, typically filtered, was collected in amber bottles for carbon isotope analyses, 60 and 30 ml samples were collected for anions and oxygen/hydrogen isotopes, respectively. Finally, a 1-L sample was collected for sulfur isotopes. Sulfur was precipitated as $BaSO_4$ by adding $BaCl_2$ in the field and filtering to collect the precipitate.

3.2. Analytical techniques

Major and minor cations (S, Si, Fe, Mg, Ca, Na, K, B, Mn, Sr, and Cu) were analyzed by inductively coupled plasma optical emission spectrometry (ICP-OES), trace elements (Li, Co, Cr, Cs, Fe, Mn, Pb, Rb, Sb, U, V, Al, Ba, Cd, Cu, Mo, As, Ni, Se, Zn, Sr, Re, Th, Y, and the REE) by mass spectrometry (ICP-MS), anions (SO_4, NO_3, Cl, Br, and F) by ion chromatography, and alkalinity by titration at the Geological Survey of Canada (1999 data) and the Geosciences Department, University of Texas at

Dallas (UTD; 2000 data). Alkalinity was thus not measured in the field, but was determined as soon as the samples were returned to Canada/US. Total alkalinity is conservative, so that loss of CO_2 from the sample bottles will not affect total alkalinity. Most samples had low Fe contents (<1 mg/L) so that precipitation of $Fe(OH)_{3(s)}$ likely had little impact on total alkalinity. Bromine and I were also measured by ICP-MS. Electrical balances are excellent with all waters showing less than 5% difference between cations and anions. Saturation indices and P_{CO_2} calculations were performed using the computer code PHREEQC (Parkhurst, 1995), utilizing the WATEQ4F thermodynamic database (Ball and Nordstrom, 1991).

Stable isotopes were measured at the Department of Earth Sciences, University of Ottawa, (oxygen, hydrogen, carbon, and sulfur) with additional sulfur isotopes measured at the Department of Physics and Astronomy at the University of Calgary. For deuterium analyses, 3 μL of sample was trapped by liquid nitrogen under vacuum (<10 mT) in Pyrex breakseals with 100 mg zinc. Samples were baked at 500 °C for 30 min before analysis on a modified Micromass 602E isotope ratio mass spectrometer (IRMS). Two standards were run for every eight unknowns and the data reduced by linear regression to account for variations in oxidation of zinc and changes in the reference gas. Oxygen isotopes were analyzed on a dual-inlet VG Isogas Sira 12 IRMS, modified to have a micro-inlet, using 1 ml sample aliquots. Samples were equilibrated with CO_2 gas for 6 h prior to analysis. However, for samples with salinities >10‰ TDS (total dissolved solids), equilibration times were increased to 36–48 h to allow for the greater hydration sheath of ions in high salinity solutions. During a typical analytical run, 16–17 samples were run with three or four standards and the data corrected by linear regression on the standards. Carbon isotopes were analyzed on the dissolved inorganic carbon (DIC). The $\delta^{13}C$ was measured by converting the DIC to CO_2 with 100% phosphoric acid (H_3PO_4) followed by cryogenic separation and analysis by mass spectrometry on a dual-inlet VG Isogas Sira 12 IRMS. Sulfur isotopes were measured by IRMS on a different dual-inlet VG Isogas Sira 12 instrument, following precipitation of sulfate as $BaSO_4$. For hydrogen analyses, reproducibility is typically better than ±2‰, for oxygen, better than ±0.1‰, for carbon, ±0.2‰ and for sulfur, ±0.5‰.

Aliquots for strontium isotope analysis were filtered through nylon 0.45 μm syringe filters to eliminate particulate matter and acidified with 3 N HNO_3. Strontium was extracted from the acid-soluble sample fraction using Sr-specific ion exchange columns. After desiccation, the Sr extract was diluted in ultrapure water and 2 μg aliquots loaded onto Tantalum filaments, pre-etched in phosphoric acid. Isotope ratios were measured using a second-order double focusing Nier–Johnson-type thermal ionization mass spectrometer. The $^{87}Sr/^{86}Sr$ values are normalized to $^{86}Sr/^{88}Sr = 0.1194$ following correction for the presence of ^{87}Rb. Precision is estimated to be ±0.000030 or better at the 95% confidence level. Reported $^{87}Sr/^{86}Sr$ results are normalized to the UTD long-term mean for NBS-987 of 0.710228 ± 0.000026.

4. Results

4.1. Major ions

Spence groundwaters span a large range in salinity. Waters along the eastern upflow (here and throughout, upflow refers to up hydraulic gradient and downflow to down hydraulic gradient) margin of the deposit have the lowest salinities, ranging from 900 to 7000 mg/L total dissolved solids (TDS). Within the deposit, groundwater in the central portion has moderately low salinity (as low as 9400 mg/L), with groundwaters in the northern and southern part of the deposit exhibiting salinities in excess of 44,000 mg/L (Table 1). Down-gradient of the deposit groundwaters attain TDS values as high as 53,200 mg/L (Fig. 2), with one sample two kilometers west of the deposit having a TDS value of 145,000 mg/L. Spence deposit groundwaters are mainly Na^+-rich, with in most cases $Ca^{2+} > Mg^{2+}$. Groundwaters are also dominantly Na^+–SO_4^{2-}- and Na^+–Cl^--type waters. Groundwaters along the eastern margin of the deposit are mainly SO_4^{2-}-rich, whereas waters within the deposit and down gradient from the deposit are Cl-rich, though sulfate contents are highest for groundwaters within the deposit (Fig. 3). Anions are dominated by chloride with all waters showing a strong trend of increasing Cl^- with TDS (not shown), similar to that shown for Na^+ (Fig. 3). There is a strong trend of increasing SO_4^{2-} with TDS, although groundwaters with the highest TDS show decreasing SO_4^{2-} contents with increasing salinity (Fig. 3). Groundwater HCO_3^- contents generally decrease with increasing TDS (with the notable exception of one sample, which has pH > 9.0). Both Br^- (Spearman Rank correlation between Br^- and TDS, $r_s, = 0.881$, $n = 51$; note all r_s values reported are significant to ⩾99% confidence) and I^- ($r_s = 0.847$, $n = 51$) increase with increasing TDS (Fig. 3). All Spence waters have anomalously elevated I/Cl and I/Br ratios compared to seawater and to saline waters from other settings (Fig. 4).

Cations are dominated by Na^+, which shows strong positive correlation with TDS ($r_s = 0.993$, $n = 51$; Fig. 3). Although Ca^{2+} ($r_s = 0.880$, $n = 51$), Mg^{2+} ($r_s = 0.977$, $n = 51$), and K^+ ($r_s = 0.827$, $n = 51$) all increase with increasing TDS, there is more scatter than with Na^+. Silica contents are generally low compared to the cations and there is a poor correlation with respect to TDS ($r_s = 0.292$, $n = 51$; this is not significant at 95% confidence).

Strontium, Rb^+, Li^+, and B^{3+} (as $B(OH)_3$) all show similar trends to the major cations. Barium differs from other trace cations in that the waters east of the deposit have generally higher Ba^{2+} contents than groundwaters within and down flow of the deposit. For most groundwaters, manganese contents are elevated within the deposit over

Table 1
Geochemistry of Spence deposit groundwaters

Sample#	00-1001	00-1002	00-1004	00-1009	00-1017	99-1001	99-1002	99-1006	99-1007	99-1010	99-1013	99-1014	99-1015	99-1016	99-1017	99-1018
Area	Within	Within	Within	Within	Within	Within	Within	Within	Within	Within	Within	Within	Within	Within	Within	Within
Easting	474531	474531	475040	474990	474874	474531	474904	474000	474500	474445	474829	474787	474874	473916	473924	475208
Northing	7480501	7480501	7481435	7479868	7481755	7480501	7480433	7479500	7479750	7479053	7481299	7481564	7481755	7478963	7479880	7482214
pH	6.81	6.75	7.52	7.46	7.33	6.37	6.18	6.03	4.73	5.08	6.99	7.25	7.27	7.3	6.57	7.35
Eh (mV)	223	−40	−276	−21	−259	169	390	57	316	0	172	190	217	152	218	235
DO (mg/L)	1.71	1.37	1.4	0.95	0.63	1.92	4.21	3.64	4.3	1.67	2.15	3.18	2.66	2.06	1.79	1.89
EC (mS/cm)	33	33.3	42.9	25.6	56.5	>20	16.3	>20	>20	>20	>20	>20	>20	>20	>20	>20
T (°C)	35.3	29.9	26.4	29.4	26.2	22.5	24.3	27.8	24	27.5	26.7	26.8	26.9	26.9	26.8	27
$\delta^{18}O_{VSMOW}$ (‰)	1.63	1.57	0.62	−0.28	5.17	1.31	−5.25	3.29		2.96	−2.85	5.35	6.55	3.57	2.79	6.92
$\delta^{2}H_{VSMOW}$ (‰)	−25.1	−26.4	−34.5	−33.1	−16	−22.8	−59.9	−22.7		−24.6	−52.1	−13.2	−13.8	−16.8	−20.8	−8.9
$\delta^{13}C_{PDB}$ (‰)	7.56	7.19	−7.51	9.39	−0.99	−1.81	−7.03	−1.71		−0.5	−9.39	−1.26	−2.62	−2.72	−2.26	0.67
$\delta^{34}S_{CDT}$ (‰)	3.6	3.3	3.8	4	2.9	3.6	3.2	3.6	3.7	3.4	3.3	2.4	2	2.9	3	2.1
mg/L																
TDS	25540	25280	24918	21374	37270	25543	12656	34466	26558	29162	19845	38410	44584	27000	27794	43105
HCO_3	108	101	145	122	142	107	29.6	25.0		164	153	111	69.6	134	199	122
Cl	7790	7752	9006	5183	16779	6915	3165	15040	6575	11205	6553	13500	17480	6990	8550	13575
SO_4	7031	7049	5686	7313	5105	8709	4913	6273	9503	7187	5012	7648	4916	9170	8850	9970
Br	10.9	10.9	11.8	8.1	22.7	8.3	2.9	22.9	7.8	15.3	7.6	14.2	20.8	8.6	12.6	13.0
I	31.9	32.1	19.6	20.1	33.1	30.3	34.2	37.6	29.3	31.1	19.7	56.9	37.1	30.3	26.8	64.3
Ca	589.2	593	726.9	499.7	1119.6	580	548	948	543	730	712	789	1306	588	598	731
Mg	289.3	290.2	244.9	182.3	467.8	232	43.5	445.9	251.2	300.4	176.4	430.2	539.2	266.1	289	302.5
Na	7743	7631.7	7756.9	6127.2	12413	8055	3794	11571	8322	9461	6023	11971	14287	8298	9132	13763
K	92	93.3	81.5	81.9	122.7	106.4	71.4	162.8	120	115.2	82.9	95.6	120.6	120.5	97.2	81
Si	6.7	6.6	8.1	5.2	7.3	7.6	15.7	20.7	33.8	6.4	10.4	9.9	6.0	15.7	7.5	10.1
B	71.5	71.4	39.6	40.8	70.7	57.7	24.1	36.5	70.8	38.5	33.1	68.3	62.7	69.8	38.7	77.5
µg/L																
Fe	31	29	46	26	97			54454		10342	872					
Mn	615	581	880	1354	235	1163	231	3948	184	563	2095	14	118	527	1923	28
Al	109	106	111	106	130	43	51	57	860	20	159	20	20	20	20	20
Ba	17	21	41	30	169	16	13	26	11	15	23	14	30	29	20	15
Cs	84	81	11	109	42	85.5	9.8	273.3	41.1	185.3	15	23.3	15.2	17.7	23	36.7
Ni	65	59	34	90	45	60	21	17	85	23	24	15	24	24	28	14
Li	5259	5298	3913	4410	5209	5716	1361	9323	5344	7327	3068	5957	7152	5433	6950	5657
Rb	214	208	116	221	253	244	123	745	294	364	151	146	168	280	374	161
Sr	7483	7281	10931	5224	18931	5796	1252	7617	6490	8858	2264	16324	22168	7022	10733	14260
U	0.39	0.42	1.86	1.89	0.68	0.5	0.4	0.1	1.8	0.8	1.8	0.1	0.7	0.5	0.8	0.3
V	28	30	41	23	75	0.6	0.1	0.2	1.3	1.9	2.4	1.1	0.4	0.5	1.6	1.4

Area	Within	Within	Within	West	West	West	West	West	West	West	West	West	West	West	East	East
Easting	474990	474200	474700	472000	472000	473451	473451	473475	473451	472500	473475	474031	472549	472521	475340	475206
Northing	7479868	7480200	7480100	7480000	7479000	7479500	7479500	7480511	7479500	7481500	7480511	7481487	7478950	7478522	7481975	7481379
pH	6.43	9.22	7.54	7.21	7.87	7.67	7.67	7.35	7.55	6.53	6.86	7.37	7.28	7.41	8.3	8.39
Eh (mV)	174	−6	66	−186	−207	−165	−165	−338	−278	−188	230	176	485	470	−341	−310
DO (mg/L)	0.89	0.28	1.01	0.58	0.79	0.82	0.82	0.92	2.58	0.63	1.85	4.61	2.56	2.3	0.8	2.8
EC (mS/cm)	>20	>20	11.56	89.8	24.5	38.4	38.4	32	38.2	240	>20	>20	>20	>20	4.97	2.09
T (°C)	26	25.4	26.3	30.6	32.2	28.7	28.7	28.2	29.4	30.8	28	29.3	24.8	24.9	28.9	21.8
$\delta^{18}O_{VSMOW}$ (‰)	−2.77	1.47	−3.38	5.24	0.76	3.69	3.61	7.37	3.66	10.71	7.25	5.88	3.23	2.92	−9.5	−10.39
$\delta^{2}H_{VSMOW}$ (‰)	−54.5	−22.9	−52.5	−21.7	−26.4	−16.3	−16	−10.1	−14.3	−5.8	−13.7	−15.4	−20.7	−18.6	−75.6	−83.3
$\delta^{13}C_{PDB}$ (‰)	0.12	−27.36	−4.36	−0.47	3.04	1.06	0.4	−3.07	0.65	−4.58	−15.55	−2.23	−3.89	−3.3	−13.14	−9.03
$\delta^{34}S_{CDT}$ (‰)	4.3	3.7	7.8	3.5	3.7	3.7		2.5	3.4	0.9	1.7	2.5	2.5	2.8	7.3	5.1
mg/L																
TDS	15719	24409	9359	54483	20114	29332	29165	39045	28757	145020	53155	39495	27594	26761	3875	1716
HCO_3	148	629	260	75.9	89.2	199	165	137	183	134	104	116	76.9	84.9	309	424
Cl	3978	7105	1731	35483	4803	9522	9457	19542	9844	80467	21150	15050	10525	8470	678	47.0
SO_4	6102	7918	4209	1983	6648	7475	7490	4706	7196	2004	4269	7001	5770	6486	1387	539
Br	5.3	9.2	2.1	55.0	7.4	14.4	15.7	25.0	15.1	78.6	26.0	17.2	12.3	11.1	0.9	0.2
I	15.7	28.2	8.9	47.3	20.2	36.0	37.1	40.4	36.8	127.3	49.3	57.8	35.8	38.5	3.6	0.6
Ca	507	558	526	3861.5	549.8	638.3	637.2	1305.6	628.6	4018	1747	885	787	711	116.9	29.9
Mg	128.9	155	48.5	1249.6	151.6	335.7	334.6	775.6	331.8	1952.9	874.1	569.8	297.3	262.7	21	3.7
Na	4777	7763	2525	17663.1	5795.5	9062.9	8998	12911.3	8917.1	52974.1	16642	12528	8309	8621	1019.2	435.4
K	74.9	138.8	58.6	145.6	50	97	96.3	180.2	94	718.3	219	94.3	93.1	85.3	30.8	19.2
Si	5.0	0.1	12.0	5.4	10.7	10.0	9.9	11.3	9.8	3.6	13.4	9.0	10.3	9.8	5.5	5.4
B	30.0	61.5	14.9	48.0	61.4	74.3	74.3	80.7	73.4	140.5	71.3	69.1	54.4	59.4	7.6	2.4
µg/L																
Fe			698	48	37	76	30	36	71	135					315	767
Mn	1456	670	801	25	6.26	15	15	504	3.53	346	162	7	2	1	132	113
Al	46	20	20	206	133	128	125	108	158	135	42	43	20	20	61	39
Ba	25	32	66	80	18	24	19	41	29	167	31	17	15	11	36	21
Cs	41.2	4.5	4.7	39	3.69	4.21	3.77	24	4.31	225	2.3	29.7	1.4	0.3	4.38	2.1
Ni	53	13	19	132	23	31	28	55	26	260	25	17	16	15	8.93	3.22
Li	3765	5141	1305	7225	2620	5603	5545	5492	5506	10056	5852	5770	4725	5467	398	195
Rb	157	122	65	236	58	143	140	175	144	813	152	159	103	68	61	36
Sr	3969	8410	1974	79088	12426	12790	12630	27854	12606	90678	35944	17553	13945	13129	868	271
U	0.3	0.1	0.1	2.75	2.41	5.61	5.51	7.01	5.33	2.52	0.3	0.1	0.1	0.1	0.05	0.92
V	3.7	0.1	3.7	143	41	60	55	83	60	263	3.9	2	4.1	3.8	3.71	3.64

(*continued on next page*)

Table 1 (*continued*)

Sample#	00-1006	00-1008	00-1013	00-1016	99-1011	99-1012	99-1019	99-1020	99-1021	99-1022	99-1029	00-1010	00-1011	00-1012	00-1022
Area	East	East	East	East	East	East	East	East	East	East	East	North	North	North	South
Easting	475206	475295	475500	475500	475206	475360	475340	475324	475295	475229	474708	476000	476500	475000	475977
Northing	7481379	7480003	7480000	7481500	7481379	7481180	7481975	7481686	7480003	7479872	7480838	7483500	7483000	7483500	7478000
pH	8.32	8.21	7.81	8.67	7.57	7.05	7.97	7.58	7.14	7.78	7.32	7.71	7.86	8.1	7.52
Eh (mV)	−254	−180	−262	−229	125	180	−314	−48	160	31	88	−228	−288	−314	−131
DO (mg/L)	3.85	0.95	1.22	2.01	1.49	3.32	0.42		1.59	1.06	0.96	1.1	1.16	1.02	0.84
EC (mS/cm)	2.04	2.75	27.5	3.86	2.44	1.32	5.05	12.4	2.83	7.61	2.96	28.3	34.3	31.9	47.7
T (°C)	26.2	29.3	28.7	28.2	27.5	26.4	27.1		26.6	26.8	26.9	29.6	25.5	29.1	28.2
$\delta^{18}O_{VSMOW}$ (‰)	−10.83	−10.82	1.76	−10.55	−10.74	−11.08	−10.83		−9.5	−8.02	−10.77	2.25	2.63	1.64	5.74
$\delta^{2}H_{VSMOW}$ (‰)	−84.1	−82.7	−17.2	−82.7	−90.6	−84.6	−79.2		−83.7	−71.3	−86.2	−23.6	−23.8	−25	−9.5
$\delta^{13}C_{PDB}$ (‰)	−9.49	−10.75	6.59	−13.78	−10.71	−13.03	−13.81		−12.73	−13.47	−13.13	−2.22	0.46	−6.03	3.63
$\delta^{34}S_{CDT}$ (‰)	5.2	5.6	3.4	5.9	4.5	5.7	4.8		5.1	4.7	3.6	3.4	3.4	3.6	3.1
mg/L															
TDS	1644	2237	24073	3087	1412	902	3395		1900	6377	2238	27351	29478	32973	34434
HCO_3	315	214	274	377	310	152	257		181	274	154	223	328	413	258
Cl	139	173	4809	379	131	49.9	595		170	1027	162	7569	7368	6197	12973
SO_4	533	920	8847	1096	524	410	1378	3945	920	2855	1204	8721	10045	9940	7256
Br	0.2	0.3	7.3	0.4	0.4	0.1	1.1		0.4	1.2	0.3	11.2	10.4	9.0	0.0
I	0.6	0.4	21.4	1.0	2.0	0.9	5.5		1.3	7.3	1.0	36.2	53.1	19.2	0.0
Ca	28.6	46.1	505.9	99.2	25	92	120	402	47	256	172	524.8	512.5	471.3	739.8
Mg	3.7	6.6	217.9	8.9	2.7	6.2	19.4	75.3	5.8	32.5	10.2	335.8	272.9	438	369.4
Na	428.2	574.7	6761.1	784.5	398	165	994	2853	564	1800	499	8066.2	8590.9	9977.4	11072.2
K	19.2	12.6	90	33	20	26.3	31.1	75.2	13	35.7	36.5	57.3	55.6	54.5	117
Si	5.4	4.1	21.5	8.2	6.2	8.4	5.8	11.7	4.5	3.3	10.3	7.8	9.4	8.1	12.0
B	2.3	5.1	78.0	3.9	2.6	1.8	8.0	20.8	5.0	16.1	3.3	51.9	78.7	14.9	86.6
μg/L															
Fe	759	4	20	669	576			1055		843	962	52	16	11	27
Mn	110	193	13	440	88	515	152	832	216	604	330	9.43	60	92	50
Al	39	23	123	46	40	41	20	231	20	20	60	133	120	22	128
Ba	19	15	23	41	16	22	47	49	12	69	34	20	22	15	23
Cs	2.08	2.9	41	0.61	1.8	0.5	4.8	3.2	2.6	2.7	0.8	89	33	100	23
Ni	4.02	5.94	26	4.44	2	5	6	17	6	76	6	19	19	16	29
Li	200	400	4913	252	171	144	368	1431	362	1082	210	4504	5028	3975	7784
Rb	36	22	175	45	32	28	57	97	20	45	48	183	145	138	194
Sr	252	375	7962	649	191	345	838	3348	342	1798	876	10424	9560	10899	15593
U	0.9	3.28	0.71	0.46	0.1	0.1	0.1	0.1	0.1	0.1	0.1	11.98	13.58	18.46	18.85
V	3.11	1.79	36	7.17	0.8	0.1	0.3	0.6	2.7	5.6	0.8	40	40	25	62

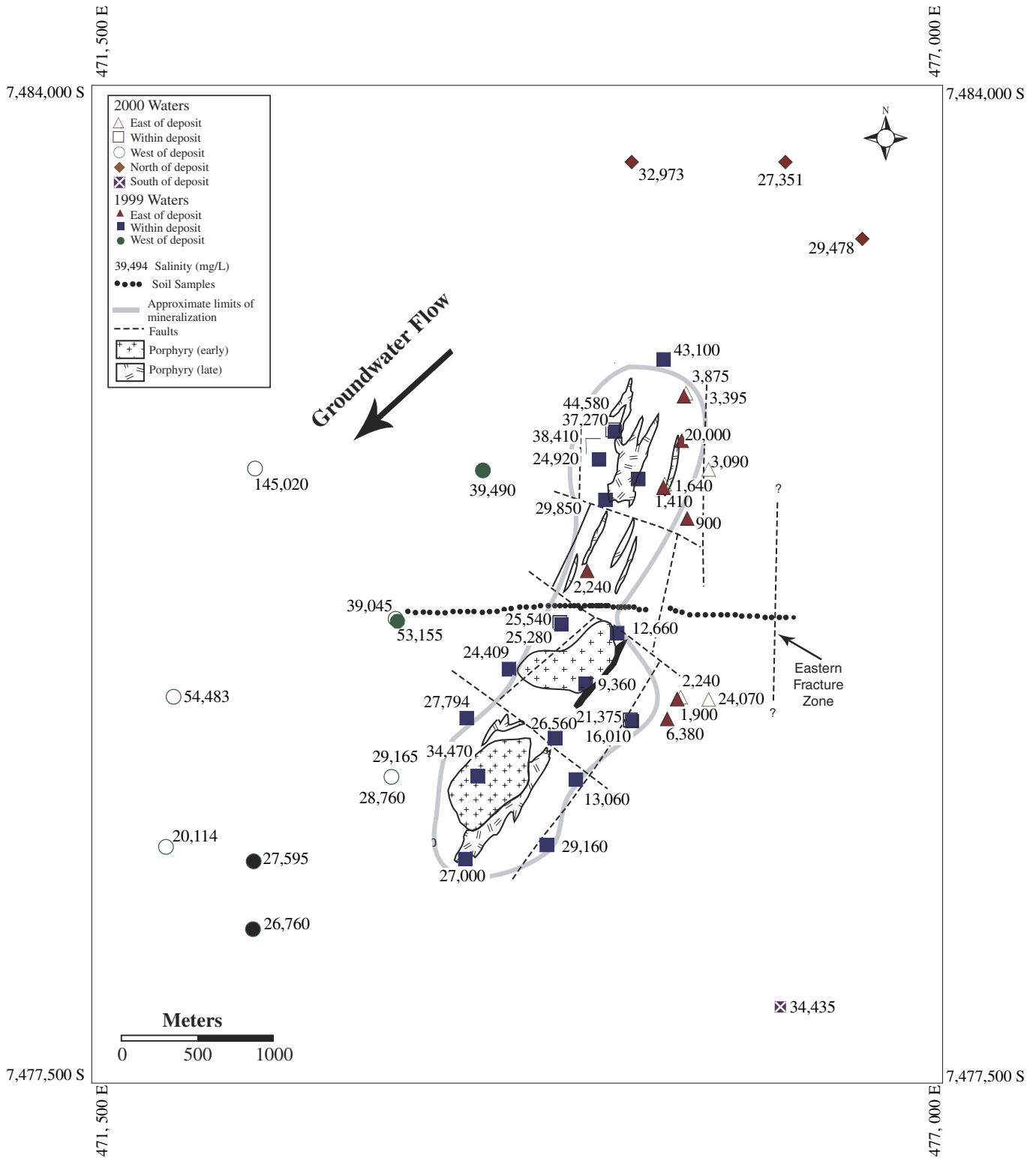

Fig. 2. Outline of the Spence deposit, showing the location of the major porphyries that intrude andesitic volcanic rocks. Also shown are the locations of groundwater samples and their salinities in mg/L total dissolved solids. Groundwater flow is generally NW to SE.

groundwaters from up-gradient of the deposit. Generally, the most elevated manganese concentrations occur along the western margin of the deposit. However, groundwaters down flow of the deposit have the lowest manganese contents.

4.2. Stable isotopic compositions

Both oxygen and hydrogen show a large range in isotopic composition for Spence groundwaters, ranging from $-11.08‰$ to $10.71‰$ and $-90.6‰$ to $-5.8‰$ for $\delta^{18}O_{VSMOW}$

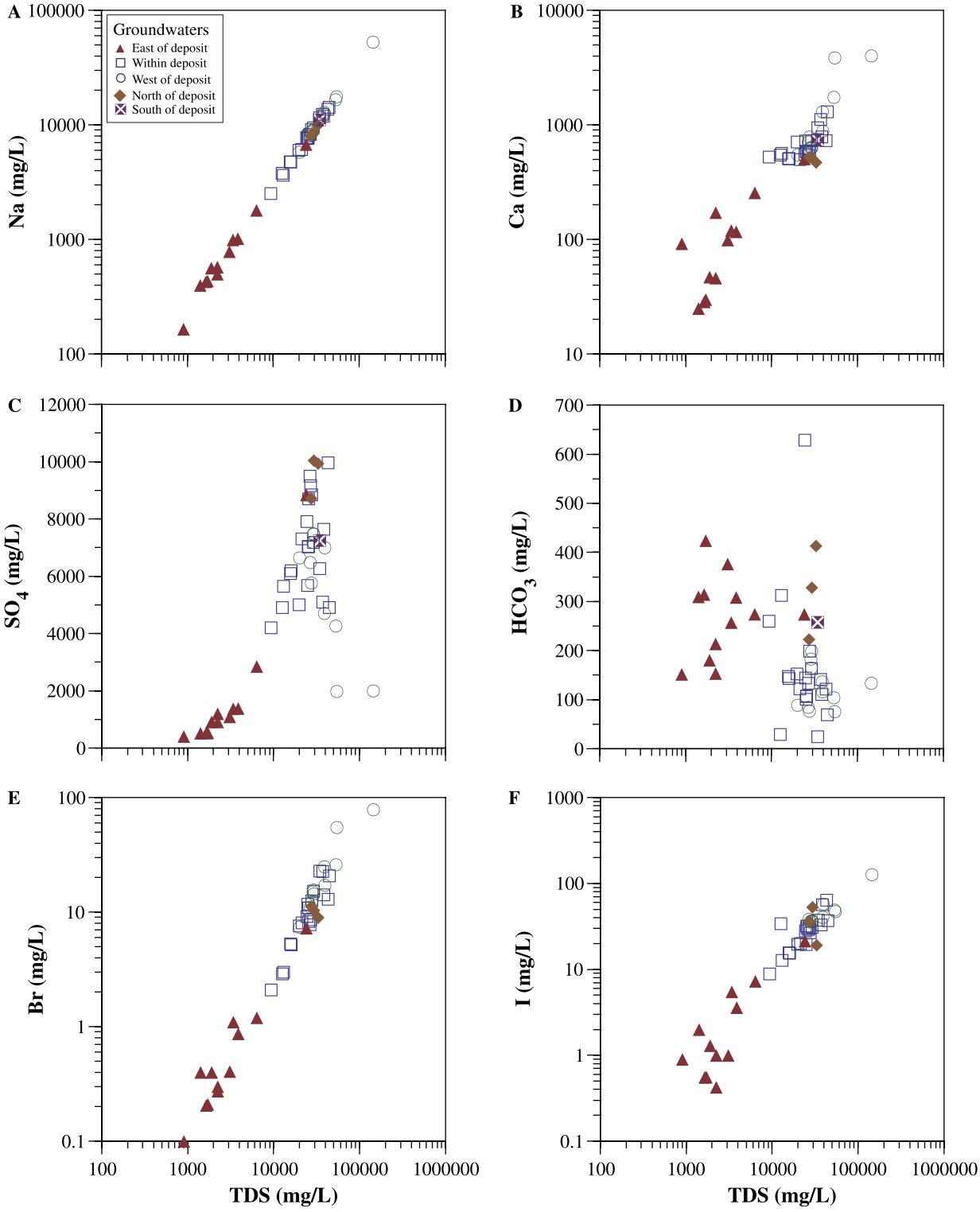

Fig. 3. Binary plots of representative major cations and anions vs salinity (total dissolved solids) for Spence deposit groundwaters, (A) Na, (B) Ca, (C) SO_4, (D) HCO_3, (E) Br, and (F) I.

and δ^2H_{VSMOW}, respectively (Fig. 5A). The most isotopically depleted waters are from the eastern upflow side of the deposit, the isotopically heaviest water is the groundwater with the highest TDS 2 km west of the deposit (Fig. 2). There is a strong positive correlation between oxygen and hydrogen isotopes with the following relationship:

$$\delta^2H_{VSMOW} = 4.31 \cdot \delta^{18}O_{VSMOW} - 36.09 (r^2 = 0.964).$$

The data form a linear array that intersects the GMWL (Global Meteoric Water Line; intersection at $\delta^{18}O_{VSMOW} = -13‰$ and $\delta^2H_{VSMOW} = -94‰$) and display a shallower slope compared to the GMWL

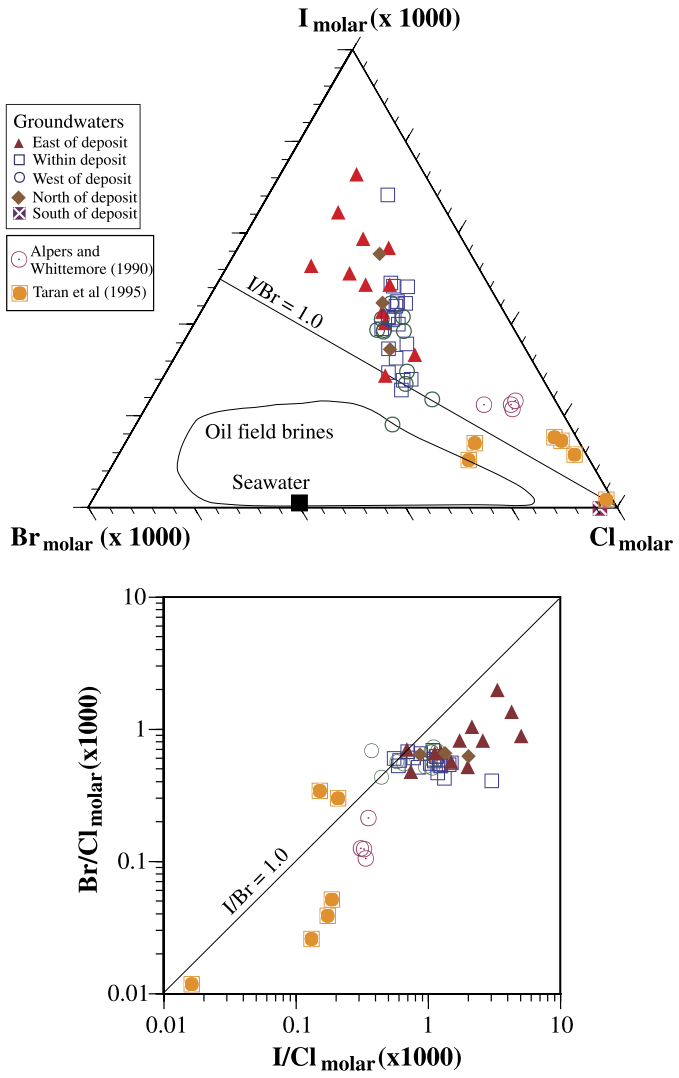

Fig. 4. Plots showing variation in Br, I, and Cl for Spence deposit groundwaters. Shown for comparison are waters from the Tamarugal anomaly (Leybourne and Cameron, in press), the Escondida mine (Alpers and Whittemore, 1990), seawater (Drever, 1997), oil-field brines (Alpers and Whittemore, 1990), and condensates of magmatic gases (Taran et al., 1995).

(Fig. 5A). The local meteoric water line (LMWL), defined on the basis of modern precipitation in northern Chile, is essentially identical to the GMWL and was defined as: $\delta^2H_{VSMOW} = 7.8 \cdot \delta^{18}O_{VSMOW} + 9.7$ (Aravena et al., 1999). The shallow slope of the Spence data is parallel to an evaporation line, for hyper arid conditions (e.g., evaporation slopes typically range from 3.9 to 4.5 for 0% to 50% relative humidity, respectively; Clark and Fritz, 1997). Both oxygen and hydrogen (not shown) become increasingly isotopically heavy with increasing salinity (e.g., Fig. 6A).

Sulfur isotopic compositions vary from +0.9‰ to +7.8‰ ($\delta^{34}S_{CDT}$), with heavier values upflow of the deposit and generally lighter values within and down flow of the deposit (Figs. 5 and 7). There is a strong negative correlation ($r_s = -0.813$; $n = 48$) between $\delta^{34}S_{CDT}$ and $\delta^{18}O_{VSMOW}$; as the isotopic composition of $\delta^{18}O_{VSMOW}$ increases, the sulfur isotopic composition decreases (Fig. 5). There is a negative, non-linear, correlation ($r_s = -0.803$ for $\delta^{34}S_{CDT}$ vs Ln(TDS); $n = 48$) between $\delta^{34}S_{CDT}$ and salinity, although there is little correlation with dissolved sulfate contents (Fig. 7).

There is a large range in $\delta^{13}C_{PDB}$, from −28.4‰ to +9.39‰ (Figs. 5 and 8). Moderately alkaline, near-neutral pH waters at the eastern edge of the deposit have $\delta^{13}C_{PDB}$ values that range from −10‰ to −15.5‰. Most of the waters within and down flow of the deposit have more elevated $\delta^{13}C_{PDB}$ values, up to 9.39‰. These isotopically enriched waters also have lower alkalinity than more depleted (with respect to carbon isotopes) waters. The groundwater with the $\delta^{13}C_{PDB}$ value of −27.4‰ also has the highest alkalinity (516 mg/L) and pH (9.22). There is a positive correlation for most waters (except the high pH water) between carbon isotope composition and sulfate content. There is little correlation between $\delta^{13}C_{PDB}$ and either pH or dissolved inorganic carbon (HCO_3^-), and there is a weak positive, non-linear correlation with salinity (Fig. 8). In general, groundwaters with the highest $\delta^{13}C_{PDB}$ values have the lowest $\delta^{34}S_{CDT}$ (Fig. 5D).

4.3. Speciation and mineral saturation

Groundwaters (filtered aliquots) were speciated and mineral saturations calculated using the computer code PHREEQC (Parkhurst, 1995), using the WATEQ4F thermodynamic database (Ball and Nordstrom, 1991). Determination of mineral saturation indices reveals several significant features of the Spence deposit groundwaters. The Saturation Index (SI) is defined as:

$$SI = \log(IAP/K),$$

where, IAP is the ion activity product and K is the equilibrium constant.

All low salinity waters east of the deposit are undersaturated with respect to gypsum, whereas all groundwaters within the deposit and west of the deposit are saturated to supersaturated with respect to gypsum. The decrease in SO_4^{2-} at the highest TDS contents noted above may indicate that SO_4^{2-} contents are controlled in part by formation of gypsum. None of the groundwaters are close to halite saturation, although SI_{halite} increases with increasing Na and Cl contents. Essentially, all of the waters are at or well above barite saturation, although SI_{barite} decreases with increasing SO_4^{2-} contents. All groundwaters are undersaturated with respect to $CO_{2(g)}$, although many waters have P_{CO_2} contents greater than atmospheric (P_{CO_2} ranges from $10^{-5.43}$ to $10^{-1.51}$, atmosphere = $10^{-3.5}$).

Several groundwaters are at or above calcite saturation, although several groundwaters with elevated SO_4^{2-} contents are well below calcite saturation, and also possess carbon isotopic compositions close to and greater than 0‰

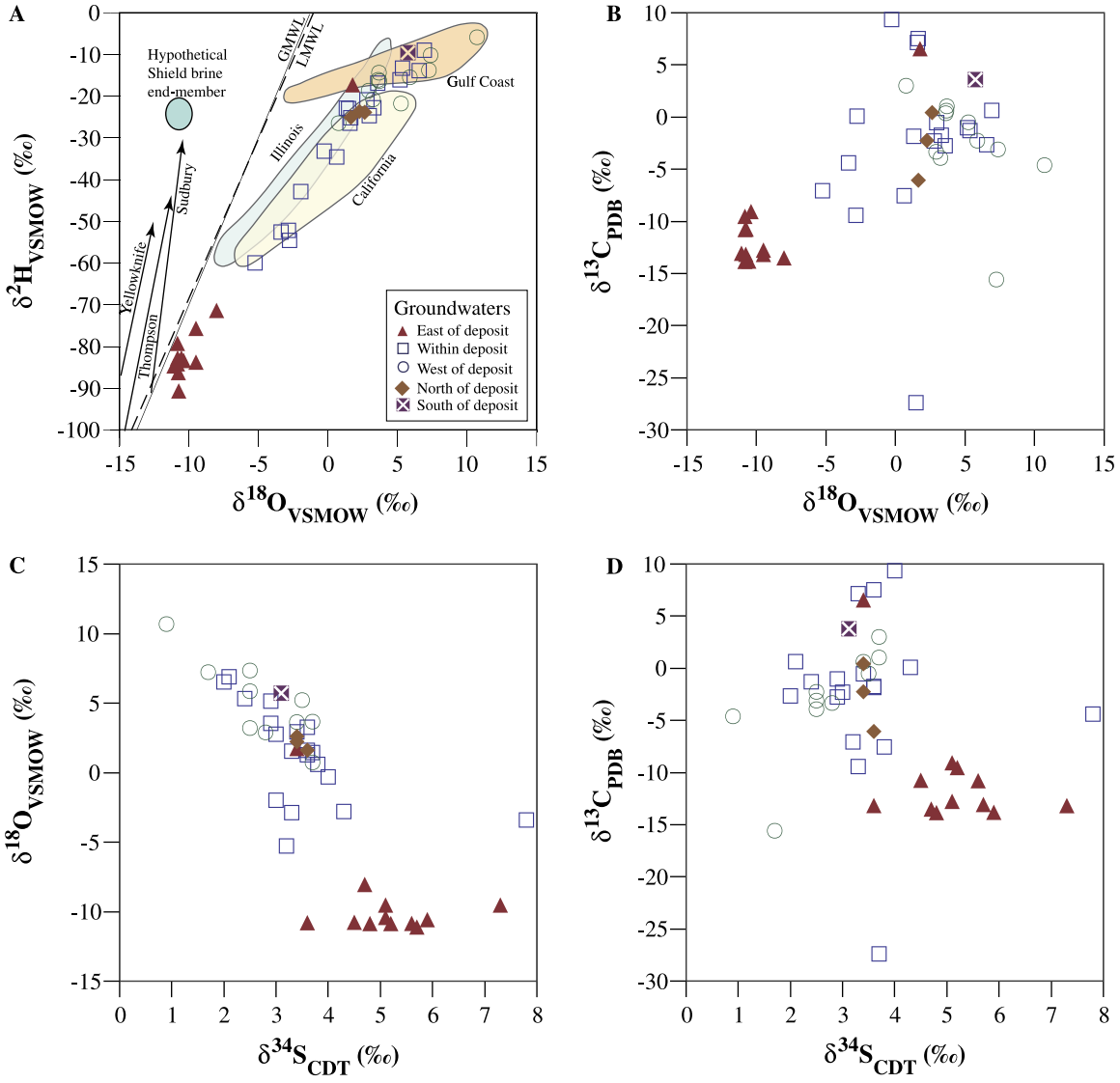

Fig. 5. Binary plots of stable isotopic compositions of Spence groundwaters. (A) δ^2H_{VSMOW} vs $\delta^{18}O_{VSMOW}$. GMWL, global meteoric water line of Craig (1961); LMWL, local meteoric water line after Aravena et al. (1999). Also shown are fields for sedimentary basin brines (Gulf Coast, Illinois, California) from (Hoefs, 2004; Taylor, 1974) as well as trends for shield brines from Thompson, Yellowknife, and Sudbury and the hypothetical end-member for Canadian shield brines after (Bottomley et al., 1999; Frape et al., 1984). (B) $\delta^{13}C_{PDB}$ vs $\delta^{18}O_{VSMOW}$. (C) $\delta^{18}O_{VSMOW}$ vs $\delta^{34}S_{CDT}$. (D) $\delta^{13}C_{PDB}$ vs $\delta^{34}S_{CDT}$.

PDB. Additionally, $SI_{calcite}$ decreases sharply at high Ca^{2+} contents and for waters above gypsum saturation. Several waters within the deposit are well above alunite saturation, which may be controlling K^+ contents.

4.4. Strontium isotopes

Strontium isotopes were determined on 14 groundwaters from the 1999 data set. Strontium isotopic compositions range from $^{87}Sr/^{86}Sr = 0.708423$ to 0.709299 (Fig. 9). There is almost complete overlap between waters from upflow, within and down flow of the deposit. There are no obvious trends in the strontium isotope data relative to Sr^{2+}, Rb/Sr, or stable isotopes, although there is a subtle negative correlation with Sr/Ca ratios (Fig. 9).

5. Discussion

5.1. Dominant controls on groundwater compositions

Groundwaters upflow of the deposit are characterized by relatively low salinities and Na–Ca–SO_4-type compositions. In contrast, groundwaters recovered within the deposit and down flow of the deposit are characterized by elevated salinities (up to and in excess of seawater salinity) and are dominantly Na–Cl-type waters (Fig. 3). There are three possible explanations for the enhanced salinity of the groundwaters within the vicinity of the deposit: (1) evaporation; (2) mixing between dilute and saline waters; and (3) dissolution of salts. It seems unlikely that dissolution of salts should occur fortuitously within the confines of the deposit. Therefore, we suggest that one or both of

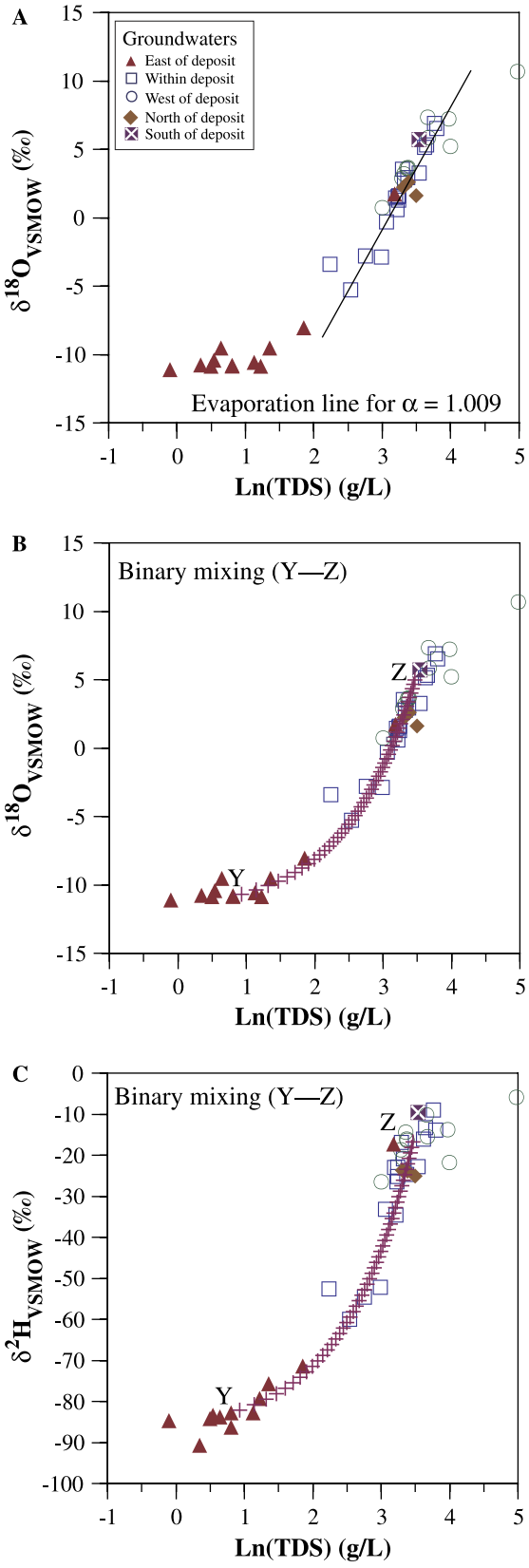

Fig. 6. Plots of Ln salinity vs $\delta^{18}O_{VSMOW}$ and $\delta^{2}H_{VSMOW}$ showing models for (A) evaporation and (B, C) binary mixing for Spence deposit groundwaters. For mixing models, tick marks are given at 2% intervals. The mixing model better accounts for the variation in the entire data set, although many of the saline waters are can be modeled by evaporation.

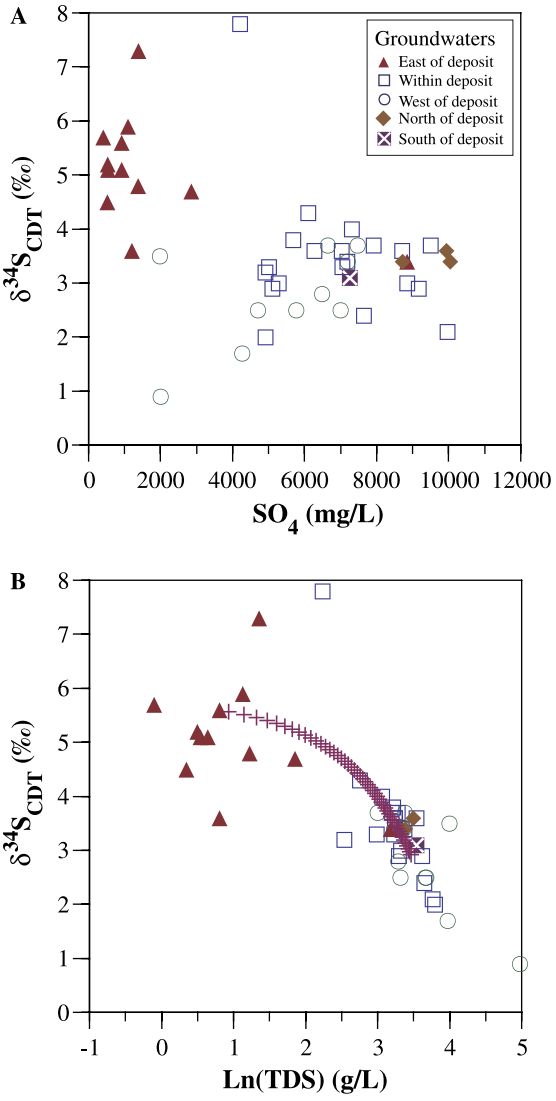

Fig. 7. Plots of (A) Ln salinity and (B) SO_4 vs $\delta^{34}S_{CDT}$ for Spence deposit groundwaters. Also shown is the effect of mixing between saline and dilute end-member groundwaters. Tick marks at 2% mixing intervals.

the first two options is most likely, in combination with water–rock interaction (as discussed below).

The oxygen and hydrogen stable isotope data show a strong linear trend with a shallow slope (4.31) compared to the global meteoric water line (Fig. 5) or local meteoric water line (LMWL), defined on the basis of modern precipitation in northern Chile: $\delta^{2}H_{VSMOW} = 7.8 \cdot \delta^{18}O_{VSMOW} + 9.7$ (Aravena et al., 1999). The shallow slope shown by the Spence groundwater data is similar to the expected range of slopes for an evaporation line at the low humidity of the Atacama Desert (Craig et al., 1963; Clark and Fritz, 1997). Note, however, that groundwaters collected from the Salar de Punta Negra show clear evidence for evaporation and hydrogen and oxygen isotope systematics have a somewhat steeper slope of 5.29 (Rissmann, 2003) or 4.97 (Alpers and Whittemore, 1990) for different years of collection. Alpers and Whittemore (1990) suggested that linear trends between Ln(TDS) and $\delta^{18}O_{VSMOW}$ would be consistent with

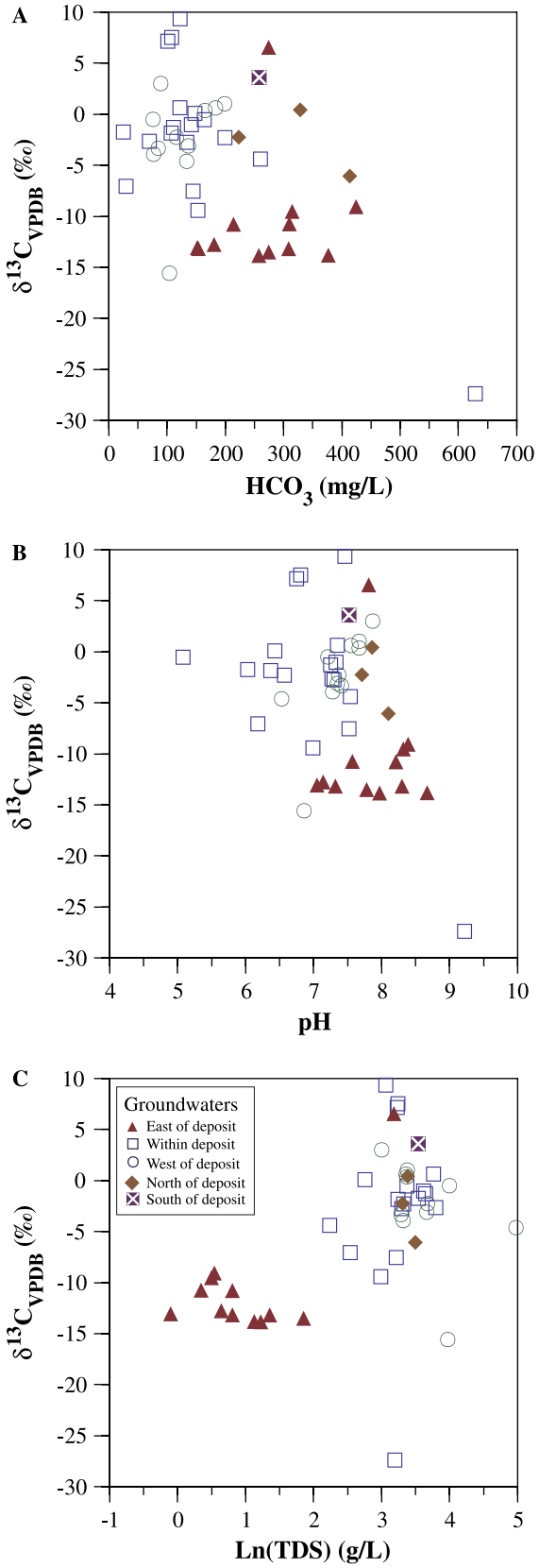

Fig. 8. Plots of $\delta^{13}C_{PDB}$ vs (A) HCO_3, (B) pH, and (C) Ln(TDS) showing the relationships between relatively dilute upflow waters compared to those in and down flow of the Spence deposit. Note that waters interacting with porphyry mineralization have elevated salinity and heavier carbon isotope compositions than dilute upflow waters.

evaporation. However, although segments of Ln(TDS) vs $\delta^{18}O_{VSMOW}$ are straight for the Spence deposit (Fig. 6A), no linear relationship exists between the low salinity waters along the eastern margin of the deposit and those within or down flow of the deposit, and the most saline waters also deviate from a simple evaporation line. The lack of a linear relationship indicates that the high salinity waters within the deposit are not merely the product of evaporation of the upflow waters. Thus, although theoretically the shift in $\delta^{18}O_{VSMOW}$ and $\delta^{2}H_{VSMOW}$ is consistent with an evaporation trend and would also generate increasing salinity with isotope fractionation (Fig. 6A), not all of the variation can be explained by evaporation. It is also difficult to imagine how approximately 75% evaporation fortuitously occurs within the immediate vicinity of the Spence deposit. It may be that there is a component of evaporation, but trends for many elements suggests that mixing between waters is dominant. Note also that there is an inflection (albeit subtle) to lower slope for the isotopically heaviest waters (i.e., the 14 most saline waters have a slope of 1.47; Fig. 5A).

If evaporation were the main process controlling the increase in salinity, constant ratios between conservative tracers and Cl^- with increasing salinity would be expected. However, with increasing Cl^-, Na/Cl, and Li/Cl ratios decrease and are more consistent with groundwater mixing (e.g., Na/Cl vs Cl^-; Fig. 10). In addition, there are strong correlations between major ions and oxygen isotopic composition, suggesting that the trend in stable oxygen and hydrogen isotopes (Fig. 5A) is a mixing line. We have used simple two-component mixing to model the isotopic and geochemical variation in the Spence groundwaters. Although this modeling does not produce perfect fits (not an unexpected result for simple binary mixing), mixing between relatively fresh and saline end-members does conform reasonably well to the variation in oxygen and hydrogen isotopes with salinity (Figs. 6B and C). Indeed, binary mixing produces a better fit to the oxygen and hydrogen data than does evaporation (Fig. 6). Although the fit is not as good, binary mixing can also explain much of the variation in sulfur isotopic composition with salinity (Fig. 7B). Evaporation should have no effect on the S-isotopic composition of Spence groundwaters, as gypsum precipitation (or the formation of other sulfate minerals such as alunite) is essentially a non-fractionating process for sulfur ($\Delta^{34}S_{gypsum\text{-}brine} = +1.65 \pm 0.12‰$; Thode and Monster, 1965).

It is possible that structures responsible for controlling the location of the mineralizing fluid during formation of the porphyry sulfides at the Spence deposit are still active and provide a conduit for deep saline waters to reach the surface environment. There are prominent fracture zones in the Miocene gravels overlying the deposit, which have been interpreted as resulting from reactivation of a basement fault coincident with the deposit (Cameron et al., 2002). Such a structure may have focused the intrusion of

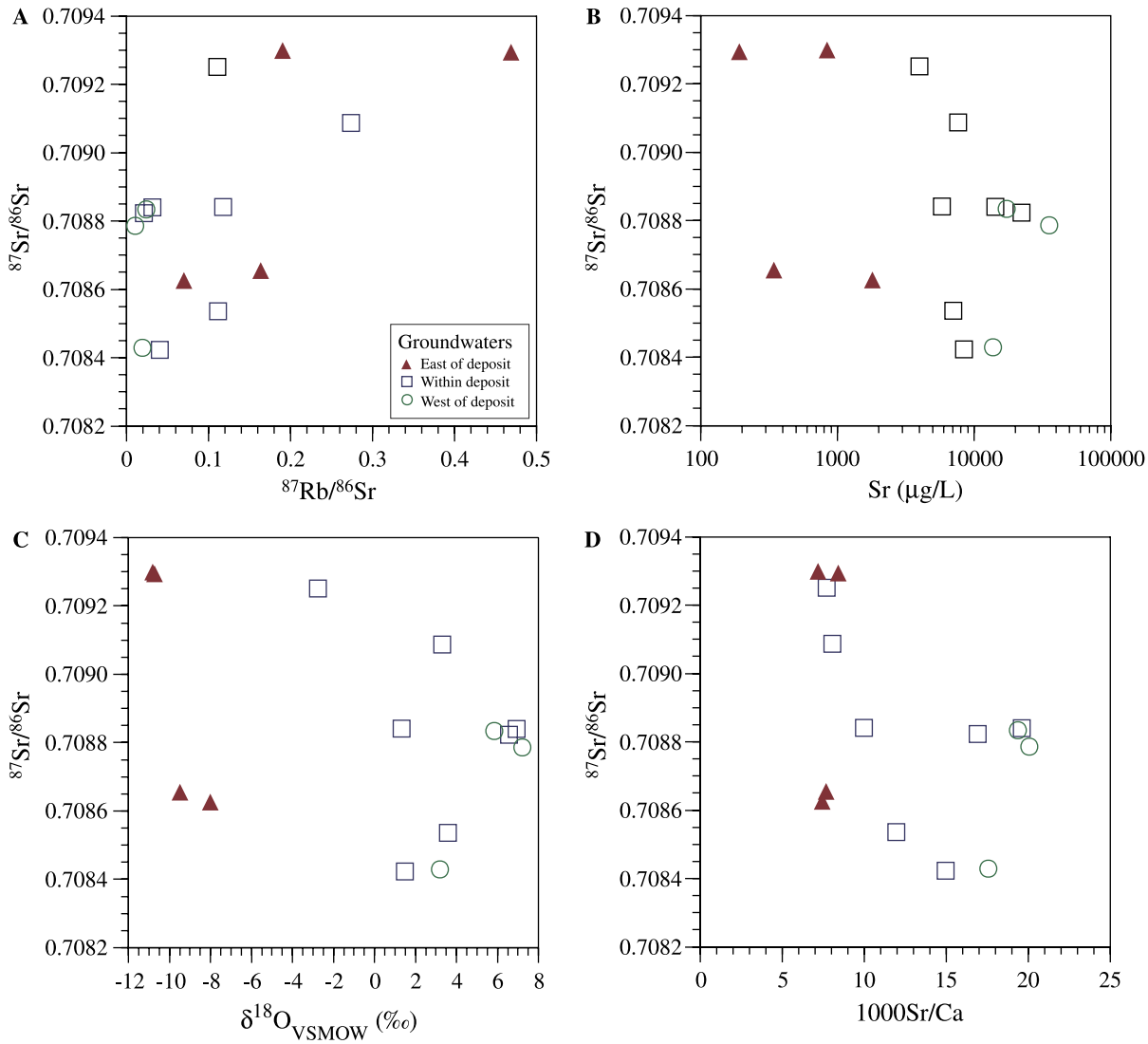

Fig. 9. Strontium isotope variation diagrams. (A) $^{87}Sr/^{86}Sr$ vs $^{87}Rb/^{86}Sr$, (B) $^{87}Sr/^{86}Sr$ vs Sr, (C) $^{87}Sr/^{86}Sr$ vs $\delta^{18}O_{VSMOW}$, and (D) $^{87}Sr/^{86}Sr$ vs Sr/Ca showing the relationships between relatively dilute upflow waters compared to those in and down flow of the Spence deposit.

the porphyries along a north-northeast trend. Within the deposit area, these deeper Na^+–Cl^- fluids interact with a more regional and shallower groundwater flow system, dominated by Na^+–Ca^{2+}–SO_4^{2-}-type waters. Elevated sulfate values in the region of the deposit are likely due to recent oxidation of massive sulfides residual from hypogene alteration in the Miocene (as suggested by the S isotope compositions, see below).

Therefore, it appears that there are several processes active at the Spence deposit. Both groundwater mixing and evaporation may be occurring, although we suggest that the former process is more important. A predominant control by evaporation is also inconsistent with the variation in Na/Cl_{molar} ratios (Fig. 10), which, given the lack of saturation for salts of Cl^- and Na^+, should not change (in the absence of significant cation exchange). In addition, there is clear evidence of water–rock reactions within the vicinity of the deposit, as shown by decreasing sulfur isotope values, loss of alkalinity and increasingly heavy $\delta^{13}C_{PDB}$ values (Figs. 7 and 8), and increased porphyry copper mineralization-related metal contents (Leybourne and Cameron, unpublished data).

Alpers and Whittemore (1990) suggested that there may be a metamorphic fluid component to the saline waters at depth at the Escondida deposit. As evidence for a metamorphic fluid influence, they showed that for the most saline waters at La Escondida, there was a greater shift in $\delta^{18}O_{VSMOW}$ than for $\delta^{2}H_{VSMOW}$. For the Spence deposit waters, the most saline waters also appear to have a slightly shallower slope than the bulk trend (Fig. 5A). Note, however, that the Spence data extends to heavier oxygen and hydrogen isotopic values compared to Escondida. These most saline waters from the Spence deposit have oxygen and hydrogen isotope compositions that are more similar to modified formation waters (i.e., modified paleoseawater) than typical metamorphic fluids (Taylor, 1974; Hoefs, 2004). The most enriched isotopic values from the Spence deposit are similar to so-called "arc-related water" from

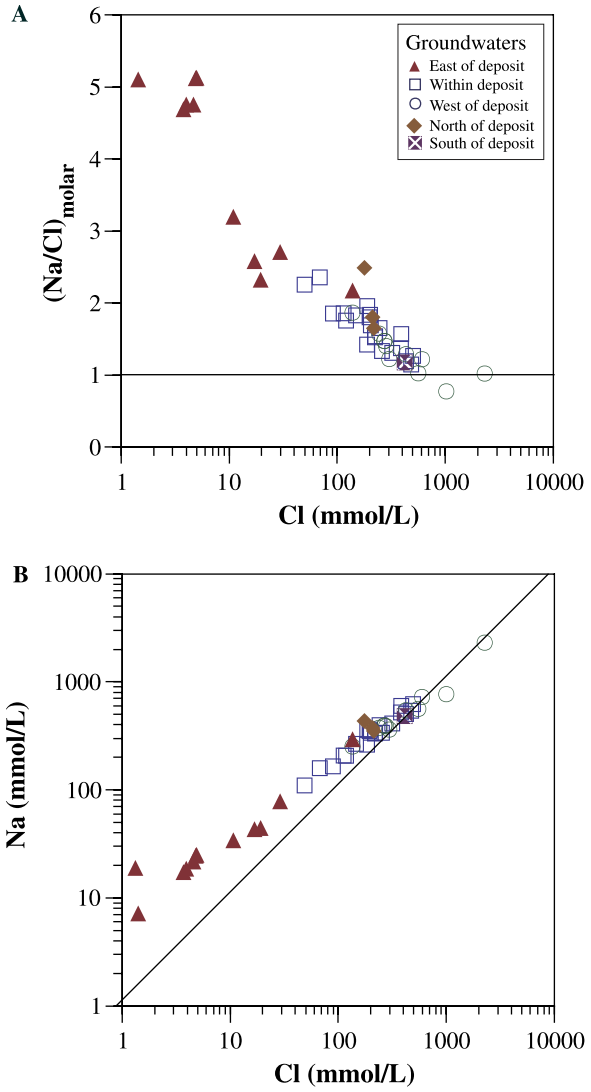

Fig. 10. Plots of (A) Na/Cl_{molar} and (B) Na vs Cl for Spence deposit groundwaters. Note that simple evaporation would not change the Na/Cl_{molar} ratio.

degassing of andesitic magmas (Taran et al., 1995; Lewicki et al., 2000).

Risacher and Fritz (1991) showed that waters from Bolivian salars with elevated Cl concentrations (>~5 mM Cl^-) had $Na/Cl_{molar} = 1$, indicating dissolution of older halite evaporites. For the Spence groundwaters, all but two samples have $Na/Cl_{molar} > 1.1$ (Fig. 10), suggesting that dissolution of halite salts is less important in controlling the major solute contents of these waters. In addition, log(Cl/Br) ratios are uniform in Spence saline waters ($\log(Cl/Br = 3.26 \pm 0.06)$), lower than would be expected for halite dissolution (halite $\log(Cl/Br \sim 6$; Risacher et al., 2003)).

There are two possible explanations for the "hook" in the sulfate concentrations vs salinity (Fig. 3): (1) formation of sulfate minerals has resulted in decreasing sulfate abundance as salinity increases (likely minerals include gypsum and alunite; Na-sulfate minerals such as mirabilite and thenardite are well below saturation for all waters); and (2) alternatively, groundwater mixing may be more complicated than simple two-component mixing. This latter alternative is most likely and may also help explain the spread in the sulfate-$\delta^{34}S_{CDT}$ data (Fig. 7). Given that the SO_4/Ca ratios are all >1, precipitation of Ca-sulfates should result in preferential loss of calcium relative to sulfate. There is strong evidence that saline waters are actively interacting with sulfide mineralization in the Spence porphyry copper deposit. Evidence for a contribution from water–rock interaction includes the increasingly light sulfur isotope ratios into and downflow of the deposit, and the correlations between porphyry-related species (e.g., Se, Re, Mo, and As) and sulfur isotope ratios (Leybourne and Cameron, unpublished data). The relationship of lighter sulfur isotope ratios as Se increases is consistent ($r_s = -0.775$, $n = 39$) with oxidation of hypogene and/or supergene sulfides in and around the Spence deposit. Although the inflection in SO_4^{2-} contents with increasing salinity is unlikely to be controlled by gypsum saturation, the subtle plateau in Ca^{2+} contents at moderate salinity may be an artifact of loss of Ca^{2+} through gypsum precipitation, also suggested by the trend of increasing Mg/Ca_{molar} with salinity ($r_s = 0.832$, $n = 51$; not shown).

5.2. Groundwater sources

Based on the above discussion, much of the isotopic and compositional spread in the data is best explained by mixing of saline and dilute groundwaters. In this section, we consider the origins of these two end-member groundwaters. Previous studies of dilute groundwaters in the Atacama Desert suggested that recharge dominantly takes place in the high Andes, generally above 3500 m elevation, based on present day precipitation patterns and amounts (Fritz et al., 1981; Magaritz et al., 1990). The least saline fluids from the Spence deposit area have stable isotopic compositions that are relatively close to the GMWL and LMWL (Fig. 5A). Their compositions (−11‰ to −9‰ for $\delta^{18}O_{VSMOW}$ and −90‰ to −80‰ for δ^2H_{VSMOW}) are consistent with recharge in the Andes at elevations around 3500–4000 m (Aravena et al., 1999). Rissmann (2003) suggested that dilute groundwaters in the Monturaqui Basin, proximal to the Andes, may have been recharged at elevations lower than 3500 m during wetter periods in the Pleistocene (54.4–15.3 ka) and short periods in the Holocene (11.4–10.2 and 6.2–3.5 ka) (Bobst et al., 2001) (Houston and Hart, 2004).

The saline end-member, as discussed above, likely represents older fluids that have been transmitted along deep structures that pass through the Spence deposit; thus the regional meteoric waters mix with this saline end-member in proximity to the deposit. Fault control over the transmission of saline fluids was also suggested by Magaritz et al. (1990) for the Pampa del Tamarugal, a large inland basin to the north-northwest of the Spence deposit. There are a number of possible sources of the saline (Na–Cl-rich) end-member fluid: (1) dissolution of halite salts in the deep

subsurface; (2) recharge of playa brines generated by evaporation of more dilute inflow waters, at higher elevation (Risacher et al., 2003); (3) mixing with metamorphic fluids, as suggested for saline waters at La Escondida mine (Alpers and Whittemore, 1990); or (4) connate waters trapped during deposition of marine sediments (i.e., sedimentary basin brines). Dissolution of halite is unlikely to be significant, owing to the Cl/Br_{molar} ratios being significantly different from halite, although the most saline waters at the Spence deposit have Na/Cl_{molar} ratios similar to halite (Fig. 10). Although there are some similarities between the more saline waters at the Spence deposit and salars in the Altiplano (Risacher et al., 2003), based on the sulfur isotopes (see below), we do not consider recharging of brines from saline lakes at higher elevation to be significant; such a model would require regional flow for both the dilute (meteoric) and saline end-members. Although we cannot discount a deep metamorphic fluid as a potential end-member fluid, we note that the most saline fluids at La Escondida reported by Alpers and Whittemore (1990) show a mixing trend to a metamorphic fluid with a composition of around $\delta^{18}O_{VSMOW} = +7.0‰$ and $\delta^{2}H_{VSMOW} = -40.0‰$, values that are consistent with metamorphic fluids, but considerably lighter than the most saline fluids at the Spence deposit (Fig. 5A). However, the most saline waters from the Spence deposit have oxygen and hydrogen isotope compositions that are very similar to those expected from sedimentary basin brines (Fig. 5A). Thus, our preferred interpretation for the source of the saline end-member is connate marine water, subsequently modified through low water–rock ratio interaction at elevated temperatures with carbonates and marine clays (Clayton et al., 1966; Clark and Fritz, 1997).

Without radiogenic age dating, it is not possible to constrain the age of the saline end-member other than to suggest that the saline waters are likely old, perhaps on the order of millions of years, by analogy with shield and basinal brines in other parts of the world (Davisson and Criss, 1996; Bottomley et al., 1999; Starinsky and Katz, 2003; Gascoyne, 2004).

5.3. Carbon isotopes

In temperate climates, groundwater carbon isotope compositions reflect a mixture of DIC from dissolution of soil zone CO_2 (with $\delta^{13}C_{PDB}$ compositions of around $-20‰$ to $-22‰$ for C3-type vegetation) and weathering of carbonates (with $\delta^{13}C_{PDB}$ around $0 \pm 2‰$). Increase in $\delta^{13}C_{PDB}$ that comes with carbonate weathering is coincident with an increase in alkalinity (i.e., $H_2CO_3 + CaCO_3 = Ca^{2+} + 2HCO_3^-$). Vegetation of the high Andes is mainly C3-type plants, constraining soil zone $\delta^{13}C_{PDB}$ values to $-18‰$ to $-22‰$ (Valero-Garces et al., 1999). However, given the paucity of vegetation in the Andes (Fritz et al., 1981) their influence on the carbon isotopic composition of meteoric waters is likely to be minimal.

Groundwaters at Spence are characterized by $\delta^{13}C_{PDB}$ that range from $-15‰$ to $+10‰$ and show a weak negative correlation with carbonate alkalinity and pH (Fig. 8). It is possible that isotopically heavier groundwaters within the deposit have lower pH and alkalinity due to generation of acidity through oxidation of Fe-sulfides and subsequent oxidation of ferrous to ferric iron. An increase in acidity could cause dissolution of carbonate, raising the $\delta^{13}C_{PDB}$, as well as lowering the pH. The most likely explanation then, for the increasing $\delta^{13}C_{PDB}$ ratios and decreasing alkalinity, combined with increasing sulfate contents and decreasing sulfur isotope values is that there is ongoing oxidation of sulfide minerals. There is a reasonably strong colinearity between carbon and sulfur isotopes such that the waters with the heaviest carbon isotopes have the lightest sulfur isotopic compositions (Fig. 5D). Although carbon isotope values could conceivably become isotopically heavier during evaporation (Potter et al., 2004), evaporation would also produce increased Ca^{2+} and HCO_3^- and therefore increased $SI_{calcite}$. In fact, the groundwaters with the heaviest carbon isotope values have lower $SI_{calcite}$. Finally, if evaporation were the dominant control over groundwater composition, the groundwaters would be expected to be in equilibrium with atmospheric CO_2, whereas most of the groundwaters have P_{CO_2} less than atmospheric.

An alternative mechanism to produce isotopically enriched DIC is via biologically mediated processes of methanogenesis involving either acetate fermentation (Reaction 1; Carothers and Kharaka, 1980) or CO_2 reduction (Reaction 2; Clark and Fritz, 1997), which derive from preferential metabolism of ^{12}C:

$$CH_3COO^- + H_2O \Longleftrightarrow HCO_3^- + CH_4 \quad (1)$$

$$CO_2 + 4H^+ \Longleftrightarrow CH_4 + 2H_2O \quad (2)$$

The fractionation factor imparted is large and varies as a function of temperature (i.e., 70‰ at 25 °C; Bottinga, 1969). Reaction 1 results in an increase in DIC with increasing heavy carbon isotope values, whereas, reaction 2 results in a loss of DIC as carbon isotopic values become heavier. Examples of isotopically heavy DIC produced via biogenically mediated methanogenesis include oil field brines from California and Texas with $\delta^{13}C_{PDB}$ values as high as $+27.8‰$ (Reaction 1; Carothers and Kharaka, 1980), brackish groundwaters from the St. Lawrence Lowlands, Canada, with $\delta^{13}C_{PDB}$ values as high as $+31.6‰$ (Reaction 2; Clark and Fritz, 1997), and saline waters from around a massive sulfide deposit in eastern Canada with $\delta^{13}C_{PDB}$ values up to $+12‰$ (Reaction 2). Given that waters with the heaviest carbon isotope composition at Spence have among the lowest DIC contents, methanogenesis via CO_2 reduction is possible. However, if methanogenesis is responsible for the heavier carbon isotope ratios in Spence groundwaters, these reactions must be taking place at greater depth under conditions more reducing than those encountered during collection of the groundwa-

ters. Alternatively, degassing of CO_2 will produce progressively heavier carbon isotope values, with preferential loss of ^{12}C (Valero-Garces et al., 1999; Michaelis et al., 1985).

5.4. Sulfur isotopes

Rech et al. (2003) showed that sulfur and strontium isotopes of soil gypsum and calcite in three transects from the coast towards the Andes in the Atacama Desert were indicative of a dominantly oceanic source for Ca^{2+} and SO_4^{2-} at elevations below 1300 m and within 90 km of the coast. Further inland and at higher elevation Ca^{2+} and SO_4^{2-} in soils are mainly derived from redistributed salts from salars, which in turn are produced by evaporating groundwater. Thus, soils heavily influenced by marine aerosols (primarily by coastal fogs) have $\delta^{34}S_{CDT} > 14‰$ and $^{87}Sr/^{86}Sr > 0.7083$, values approaching modern seawater ($^{87}Sr/^{86}Sr = 0.7091$; Burke et al., 1982; $\delta^{34}S_{CDT} = 20.9‰$; Claypool et al., 1980; Rees et al., 1978). In contrast, soil gypsum influenced by dust originating in salars has $\delta^{34}S_{CDT}$ values between +5‰ and +8‰ and $^{87}Sr/^{86}Sr$ between 0.7070 and 0.7076. Salars and rare streams in the Atacama have average $\delta^{34}S_{CDT}$ of $5.4 \pm 2‰$, with a range of 2.9–8.7‰ (Rech et al., 2003) and waters and sulfates from the Salar de Atacama range from $5.9 \leqslant \delta^{34}S_{CDT} \leqslant 9.0‰$ and $0.70706 \leqslant {}^{87}Sr/^{86}Sr \leqslant 0.70857$ (Carmona et al., 2000). Similarly, groundwaters from in and around the Salar de Punta Negra, near Mina Escondida, have $\delta^{34}S_{CDT}$ from +3.0‰ to +8.3‰ (Rissmann, 2003). The Central Depression hosts remnants of the Hilaricos and Soledad formations (Upper Miocene and Pliocene continental evaporites) that have $\delta^{34}S_{CDT}$ compositions between +4.5‰ and +9‰, consistent with an origin dominantly from volcanic influences (Pueyo et al., 2001). The characteristically positive and relatively homogenous isotopic signatures for dissolved sulfate and gypsum/anhydrite in groundwaters and salars of the Atacama Desert have been attributed to the isotopic enrichment of sulfate during the oxidation of sulfur in shallow epithermal systems (Pueyo et al., 2001).

The sulfur isotopic systematics are best interpreted as mixing between the dilute regional groundwaters flowing into the deposit from the east, with $\delta^{34}S_{CDT}$ typical of the interior of the Atacama Desert and recharge in the high Andes (+4.5‰ to +9‰), and lighter sulfur derived from (a) the more saline (formation) waters; and (b) dissolution of hypogene/supergene sulfides in the deposit. There is no data to date on the isotopic composition of hypogene sulfides or supergene sulfides and sulfates at the Spence deposit, although data are available for similar deposits in northern Chile. Hypogene sulfides at the El Tiente, La Andina, and El Salvador porphyry copper deposits, for example, have average $\delta^{34}S_{CDT}$ values of −1.0‰, −1.1‰, and −3.0‰, respectively (Field and Gustafson, 1976; Dold and Spangenberg, 2002). The same authors found supergene sulfates at El Salvador had $\delta^{34}S_{CDT}$ of −0.7‰, whereas averages of hypogene sulfates at the three deposits ranged from 10.2‰ to 11.9‰. There appears to be a relationship between decomposition of sulfides and the alkalinity/carbon isotopes, with water-porphyry copper interaction resulting in lighter sulfur isotope values and heavier carbon isotope values of saline waters at the Spence deposit.

5.5. Strontium isotopes

Strontium isotopes permit additional constraints to be placed on the various processes discussed above. Surface processes such as evaporation, precipitation or adsorption do not fractionate strontium isotopes (McArthur, 1994). The range in Sr isotopes for the more dilute waters on the eastern (upflow) margin of the deposit spans almost the entire range for those groundwaters within and down flow region of the deposit (Fig. 9). The data (Fig. 9) indicate that simple binary mixing or evaporation is not a viable mechanism to explain the range in groundwater compositions and confirm that water–rock interactions are also occurring.

There are two possible explanations for the Sr isotopic compositions: (1) mixing of dilute shallow groundwaters with more than one saline end-member with different Sr isotopic compositions; and/or (2) mixing combined with interaction with different host lithologies. Mafic and intermediate volcanic rocks in the Chilean Andes have lower Sr isotopic compositions than the Spence groundwaters ($^{87}Sr/^{86}Sr = 0.7030$–0.7079) (Trumbull et al., 1999; Viramonte et al., 1999). Ash-flow tuffs from northern Chile have variable Sr isotopic compositions, ranging from $^{87}Sr/^{86}Sr = 0.7066$ to 0.7090 (Siebel et al., 2001), similar in composition to the Spence groundwaters. Basement rocks in northern Chile and large volume ash-flow tuffs are more radiogenic than Spence groundwaters (Siebel et al., 2001). Thus, the range in the Sr isotopic composition of Spence groundwaters may reflect interaction with volcanic rocks (and derived sediments) of variable origin. Alternatively, water–rock interaction is commonly selective with respect to more soluble minerals (Leybourne and Cousens, 2005), such that the range in isotopic composition may record variable water–rock reaction.

Rech et al. (2003) modeled the variation in S and Sr isotopes of soils in the Atacama Desert by assuming relatively simple two-component mixing between solutes derived from salars/streams and those from oceanic aerosols. Waters and sulfates from Salar de Atacama are close to the salar end-member (Carmona et al., 2000). The groundwater Sr isotopes at the Spence deposit are more enriched than the salar end-member and extend to more radiogenic compositions than modern seawater. Either Spence groundwaters have some contribution from modern seawater (seawater has not had a Sr isotopic ratio as radiogenic as modern oceans since the early Paleozoic), or water–rock interaction has increased the Sr isotopic ratios of the waters, as discussed above.

5.6. Evidence from soils

If deep, saline waters are being introduced to the deposit along a fault, this introduction has important implications for exploration for copper deposits in the Atacama Desert, using soil geochemical surveys. If soil geochemical anomalies are the result of seismic pumping along fractures over the deposit and through the overlying gravels, as suggested elsewhere (Cameron et al., 2002), then the groundwater data suggests a further reason as to why these anomalies are typically dominated by Na^+ and Cl^-. Cameron et al. (2004, 2002) found that geochemical anomalies in soils over the Spence deposit were dominated by Na^+ and Cl^-. Groundwaters along the eastern (upflow) edge of the deposit are dominated by Na^+ and SO_4^{2-}, whereas groundwaters within and down flow of the deposit are Na^+–Cl^--type waters. Cameron et al. (2000) also noted a lack of stoichiometry between Na^+ and Cl^- in the soil analyses and suggested it may have been due to the difficulties inherent in analyzing Cl^- by ICP-MS. However, in the groundwaters, there is still a partial lack of stoichiometry between Na^+ and Cl^-; groundwaters along the eastern (upflow) margin of the deposit have Na/Cl_{molar} ratios between 2.5 and 5, whereas groundwaters within and down flow of the deposit have Na/Cl_{molar} ratios between 1.0 and 2.1 (Fig. 10). Water-soluble extracts of soils in the fracture zone in the gravels directly above the deposit have Na/Cl_{molar} ratios between 0.9 and 4.4 ($N = 14$) and average 2.0.

6. Conclusions

There is a large range in salinity in Spence groundwaters. Groundwaters that flow into the deposit from the east have elemental and isotopic composition similar to regional meteoric groundwaters. These upflow groundwaters have relatively low salinities (<10,000 mg/L) and Na^+–SO_4^{2-}-type compositions. The oxygen and hydrogen isotopic compositions of the upflow waters are consistent with recharge in the high Andes at 3500–4000 m elevation. Waters recovered within the deposit have higher salinities, up to 55,000 mg/L, with one outlier 2 km west of the deposit with a salinity of 145,000 mg/L, and are Na^+–Cl^--type. We interpret these higher salinity waters as deep formation waters flowing upwards along long-active faults, structures that may have originally focused intrusion of the host porphyries and subsequent hydrothermal fluids.

Major cation and anion compositional variation is primarily determined by mixing of the two groundwater types, although we cannot rule out a minor contribution from evaporation. Elemental and isotopic (S, C, Sr) data indicate that there are significant water–rock reactions taking place between the porphyry copper mineralization and the saline groundwaters, as indicated by increased porphyry-associated metal loads over conservative tracers and S isotopes.

Mixing of deeper more saline groundwaters with lower salinity regional groundwater flow has important implications for the development of saline and base metal anomalies over deeply buried deposits. Seismic pumping of groundwaters to the surface will produce geochemical anomalies over fracture conduits, producing apparent anomalies wherever fractures occur, whether they are barren or mineralized. However, anomalies directly over mineralization will have different abundances of porphyry copper indicator elements than Na–Cl anomalies elsewhere.

Acknowledgments

Alexi Ramirez of Riochilex is thanked for his assistance with much of the groundwater sampling. Daniel Salinas is especially thanked for assistance in soil sampling, groundwater sampling and Spanish lessons. Gwendy Hall, Judy Vaive, and Peter Belanger at the Geological Survey of Canada are thanked for the 1999 geochemical results, the Geochemistry Laboratory at the University of Texas at Dallas (UTD) for the 2000 data, and Nate Miller (UTD) for the Sr isotope data. Wendy Abdi (University of Ottawa) and Steve Taylor (University of Calgary) are thanked for overseeing the stable isotope analyses. Associate Editor Chen Zhu, journal reviewer Karen Johannesson and two anonymous reviewers are thanked for critical comments that greatly improved the manuscript. This is UTD Geosciences Department contribution #1038.

Associate editor: Chen Zhu

References

Alpers, C.N., Brimhall, G.H., 1988. Middle Miocene climatic change in the Atacama Desert, northern Chile: evidence from supergene mineralization at La Escondida. *Geol. Soc. Am. Bull.* **100**, 1640–1656.

Alpers, C.N., Whittemore, D.O., 1990. Hydrochemistry and stable isotopes of ground and surface waters from two adjacent closed basins, Atacama Desert, northern Chile. *Appl. Geochem.* **5**, 719–734.

Aravena, R., Suzuki, O., 1990. Isotopic evolution of river water in the northern Chile region. *Water Resources Res.* **26**, 2887–2895.

Aravena, R., Suzuki, O., Pena, H., Pollastri, A., Fuenzalida, H., Grilli, A., 1999. Isotopic composition and origin of the precipitation in northern Chile. *Appl. Geochem.* **14**, 411–422.

Ball, J.W., Nordstrom, D.K., 1991. *Users manual for WATEQ4F with revised thermodynamic database and test cases for calculating speciation of major, trace, and redox elements in natural waters.* USGS Open-File Report 91-183.

Bobst, A.L., Lowenstein, T.K., Jordon, T.E., Jordon, T.E., Godfrey, L.V., Ku, T.-L., Luo, S., 2001. A 106 ka paleoclimate record from drill core of the Salar de Atacama, northern Chile. *Palaeogeogr. Palaeoclimatol. Palaeoecol.* **173**, 21–42.

Bottinga, Y., 1969. Calculated fractionation factors for carbon and hydrogen isotopic exchange in the system calcite–carbon dioxide–graphite, methane–hydrogen–water vapor. *Geochim. Cosmochim. Acta* **33**, 49–64.

Bottomley, D.J., Katz, A., Chan, L.H., Starinsky, A., Douglas, M., Clark, I.D., Raven, K.G., 1999. The origin and evolution of Canadian Shield brines: evaporation or freezing of seawater? New lithium isotope and geochemical evidence from the Slave craton. *Chem. Geol.* **155**, 295–320.

Burke, W.A., Denison, R.E., Hetherington, E.A., Koepnick, R.B., Nelson, H.F., Otto, J.B., 1982. Variation of seawater 87Sr/86Sr throughout Phanerozoic time. *Geology* **10**, 516–519.

Cameron, E.M., Hamilton, S.M., Leybourne, M.I., Hall, G.E.M., McClenaghan, B., 2004. Finding deeply-buried deposits using geochemistry. *Geochem.: Explorat. Environ. Anal.* **4**, 7–32.

Cameron, E.M., Leybourne, M., Venegas, R.C., Vásquez, A.R., 2000. Preliminary Report: Geochemical Data for Soils over the Gaby Sur deposit, Chile. CAMIRO Deep-Penetrating Geochemistry, Phase II, 13 pp.

Cameron, E.M., Leybourne, M.I., Kelley, D.L., 2002. Exploring for deeply covered mineral deposits: formation of geochemical anomalies in northern Chile by earthquake-induced surface flooding of mineralized groundwaters. *Geology* **30**, 1007–1010.

Carmona, V., Pueyo, J.J., Taberner, C., Chong, G., Thirlwall, M., 2000. Solute inputs in the Salar de Atacama (N. Chile). *J. Geochem. Explorat.* **69–70**, 449–452.

Carothers, W.W., Kharaka, Y.K., 1980. Stable carbon isotopes of HCO_3^- in oil-field waters—implications for the origin of CO_2. *Geochim. Cosmochim. Acta* **44**, 323–332.

Chávez, W.X., 2000. Supergene oxidation of copper deposits: zoning and distribution of copper oxide minerals. *Soc.f Econ. Geol. Newslett.* **41**, 1–21.

Clark, I.D., Fritz, P., 1997. *Environmental Isotopes in Hydrogeology*. Lewis Publishers.

Claypool, G.E., Hosler, W.T., Kaplan, I.R., Sakai, H., Zak, I., 1980. The age curves of sulfur and oxygen isotopes in marine sulfate and their mutual interpretation. *Chem. Geol.* **28**, 199–260.

Clayton, R.N., Friedman, I., Graff, D.L., Mayeda, T.K., Meents, W.F., Shimp, N.F., 1966. The origin of saline waters, 1. Isotopic composition. *J. Geophys. Res.* **71**, 3869–3882.

Craig, H., 1961. Isotopic variations in meteoric waters. *Science* **133**, 1702–1703.

Craig, H., Gordon, L.I., Horibe, Y., 1963. Isotopic exchange effects in the evaporation of water: I. Low-temperature experimental results. *J. Geophys. Res.* **68**, 5079.

Cuadra, C.C., Rojas, G.S., 2001. Oxide mineralization at the Radomiro Tomic porphyry copper deposit, northern Chile. *Econ. Geol.* **96**, 387–400.

Davisson, M.L., Criss, R.E., 1996. Na–Ca–Cl relations in basinal brines. *Geochim.t Cosmochim. Acta* **60**, 2743–2752.

Development, U.C. o. S., 1997. Comprehensive assessment of the freshwater resources of the world. *Report of the Secretary General* E/CN.17/1997/9.

Dold, B., Spangenberg, J.E., 2002. Study of water-soluble sulfates in tailings profiles from porphyry copper deposits by sulfur and oxygen isotopes. In: *12th Annual Goldschmidt Conference*, pp. 189.

Drever, J.I., 1997. *The Geochemistry of Natural Waters*. Prentice-Hall.

Field, C.W., Gustafson, L.B., 1976. Sulfur isotopes in the porphyry copper deposit at El Salvador. *Econ. Geol.* **71**, 1533–1548.

Frape, S.K., Fritz, P., McNutt, R.H., 1984. Water–rock interaction and chemistry of groundwaters from the Canadian Shield. *Geochim. Cosmochim. Acta* **48**, 1617–1627.

Fritz, P., Suzuki, O., Silva, C., Salati, E., 1981. Isotope hydrology of groundwaters in the Pampa Del Tamarugal, Chile. *J. Hydrol.* **53**, 161–184.

Gascoyne, M., 2004. Hydrogeochemistry, groundwater ages and sources of salts in a granitic batholith on the Canadian Shield, southeastern Manitoba. *Appl. Geochem.* **19** (4), 519–560.

Hall, G.E.M., Vaive, J.E., Beer, R., Hoashi, M., 1996. Selective leaches revisited, with emphasis on the amorphous Fe oxyhydroxide phase extraction. *J. Geochem. Explorat.* **56**, 59–78.

Hamilton, S.M., 1999. Transport mechanisms responsible for selective leach anomalies. In: *Geoanalysis With Emphasis on selective Extractions*. Association of Exploration Geochemists, Short Course.

Hoefs, J., 2004. *Stable Isotope Geochemistry*. Springer-Verlag.

Houston, J., Hart, D., 2004. Theoretical head decay in closed basin aquifers: an insight into fossil groundwater and recharge events in the Andes of northern Chile. *Quart. J. Eng. Geol. Hydrogeol.* **37**, 131–139.

Lewicki, J.L., Fischer, T., Williams, S.N., 2000. Chemical and isotopic compositions of fluids at Cumbal Volcano, Columbia: evidence for magmatic contribution. *Bull. Volcanol.* **62**, 347–361.

Leybourne, M.I., Cameron, E.M., in press. Composition of soils and groundwaters at Pampa del Tamarugal: anatomy of a false (groundwater transported) geochemical anomaly. *Econ. Geol.*.

Leybourne, M.I., Cousens, B.L., 2005. Rare earth elements (REE) and Nd and Sr isotopes in groundwater and suspended sediments from the Bathurst Mining Camp, New Brunswick: water–rock reactions and elemental fractionation. In: Johannesson, K.H. (Ed.), *Rare Earth Elements in Groundwater Systems*. Kluwer, pp. 254–293.

Magaritz, M., Aravena, R., Peña, H., Suzuki, O., Grilli, A., 1989. Water chemistry and isotopic study of streams and springs in northern Chile. *J. Hydrol.* **108**, 323–341.

Magaritz, M., Aravena, R., Peña, H., Suzuki, O., Grilli, A., 1990. Source of ground water in the deserts of northern Chile: evidence of deep circulation of ground water from the Andes. *Ground Water* **28**, 513–517.

McArthur, J.M., 1994. Recent trends in strontium isotope stratigraphy. *Terra Nova* **6**, 331–358.

Meigh, J.R., McKenzie, A.A., Sene, K.J., 1999. A grid-based approach to water scarcity estimates for eastern and southern Africa. *Water Resources Manag.* **13**, 85–115.

Michaelis, J., Usdowski, E., Menschel, G., 1985. Partitioning of 13C and 12C on the degassing of CO2 and the precipitation of calcite-rayleigh fractionation and a kinetic model. *Am. J. Sci.* **285**, 318–327.

Núñez, L., Grosjean, M., 2003. Biodiversity and human impact during the last 11,000 years in North-Central Chile. In: Bradshaw, G.A., Marquet, P.A. (Eds.), *How Landscales Change, Vol. Ecological Studies*, vol. 162. Springer-Verlag, pp. 7–16.

Parkhurst, D.L., 1995. User's guide to PHREEQC—a computer program for speciation, reaction-path, advective-transport, and inverse geochemical calculations. U.S. Geological Survey.

Potter, J., Siemann, M.G., Tsypukov, M., 2004. Large-scale carbon isotope fractionation in evaporites and the generation of extremely ^{13}C-enriched methane. *Geology* **32**, 533–536.

Pueyo, J.J., Chong, G., Jensen, A., 2001. Neogene evaporites in desert volcanic environments: Atacama Desert, northern Chile. *Sedimentology* **48**, 1411–1431.

Ramos, V.A., 1988. The birth of southern South America. *Am. Sci.* **77**, 444–450.

Rech, J.A., Quade, J., Hart, W.S., 2003. Isotopic evidence for the source of Ca and S in soil gypsum, anhydrite and calcite in the Atacama Desert, Chile. *Geochim. Cosmochim. Acta* **67**, 575–586.

Rees, C.E., Jenkins, W.J., Monster, J., 1978. The sulfur isotopic composition of ocean water sulfate. *Geochim. Cosmochim. Acta* **42**, 377–382.

Richards, J.P., Noble, S.R., Pringle, M.S., 1999. A revised Late Eocene age for porphyry magmatism in the Escondida area, northern Chile. *Econ. Geol.* **94**, 1231–1248.

Risacher, F., Alonso, H., Salazar, C., 2003. The origins of brines and salts in Chilean salars: a hydrochemical review. *Earth-Sci. Rev.* **63**, 249–293.

Risacher, F., Fritz, B., 1991. Geochemistry of Bolivian salars, Lipez, southern Altiplano: origin of solutes and brine evolution. *Geochim. Cosmochim. Acta* **55**, 687–705.

Rissmann, C.F.W., 2003. Dilute hydrothermal fluids within the groundwaters of the Monturaqui Basin, northern Chile: the role of Volcano Socompa. M.S. University of Texas at Dallas.

Romero, H.I., 2002. The Andes in Chile: clash between economic and sustainable development. *Newsletter of the International Human Dimensions Programme on Global Environmental Change* **01/2002**, 7–9.

Romero, L., Alonso, H., Campano, P., Fanfani, L., Cidu, R., Dadea, C., Keegan, T., Thornton, I., Farago, M., 2003. Arsenic enrichment in waters and sediments of the Rio Loa (Second Region, Chile). *Appl. Geochem.* **18**, 1399–1416.

Siebel, W., Schnurr, W.B.W., Hahne, K., Kraemer, B., Trumball, R.B., van den Bogaard, P., Emmermann, R., 2001. Geochemistry and isotope systematics of small- to medium-volume Neogene-Quaternary ignimbrites in the southern central Andes: evidence for derivation from andesitic magma sources. *Chem. Geol.* **171**, 213–237.

Sillitoe, R.H., 2000. Gold-rich porphyry deposits: descriptive and genetic models and their role in exploration and discovery. *Rev. Econ. Geol.* **13**, 315–344.

Starinsky, A., Katz, A., 2003. The formation of natural cryogenic brines. *Geochim. Cosmochim. Acta* **67**, 1475–1484.

Taran, Y.A., Hedenquist, J.W., Korzhinsky, M.A., Tkachenko, S.I., Shmulovich, K.I., 1995. Geochemistry of magmatic gases from Kudryavy volcano, Iturup, Kiril Islands. *Geochim. Cosmochim. Acta* **59**, 1749–1761.

Taylor Jr., H.P., 1974. The application of oxygen and hydrogen isotope studies to problems of hydrothermal alteration and ore deposition. *Econ. Geol.* **69**, 843–883.

Thode, H.G., Monster, J., 1965. Sulfur isotope geochemistry of petroleum, evaporites, and ancient seas. *Am. Assoc. Petrol. Geol. Mem.* **4**, 367–377.

Tosdal, R.M., Richards, J.P., 2001. Magmatic and structural controls on the development of Cu ± Mo ± Au deposits. *Rev. Econ. Geol.* **14**, 157–181.

Trumbull, R.B., Wittenbrink, R., Hahne, K., Emmermann, R., Büsch, W., Gerstenberger, H., Siebel, W., 1999. Evidence for Late Miocene to Recent contamination of arc andesites by crustal melts in the Chilean Andes (25–26°S) and its geodynamic implications. *J. South Am. Earth Sci.* **12**, 135–155.

Valero-Garces, B.L., Delgado-Huertas, A., Ratto, N., Navas, A., 1999. Large ^{13}C enrichment in primary carbonates from Andean Altiplano lakes, Northwest Argentina. *Earth Planet. Sci. Lett.* **17**, 253–266.

Viramonte, J.G., Kay, S.M., Becchio, R., Escayola, M., Novitski, I., 1999. Cretaceous rift related magmatism in central-western South America. *J. South Am. Earth Sci.* **12**, 109–121.